Mononuclear and Binuclear Ruthenium(II) Complexes Containing 2,2′-Bipyridine or 1,10-Phenanthroline and Pyrazole-3,5-Bis(benzimidazole). Synthesis, Structure, Isomerism, Spectroscopy, and Proton-Coupled Redox Activity

Sujoy Baitalik,[†] Ulrich Flörke,[‡] and Kamalaksha Nag*[,†]

Department of Inorganic Chemistry, Indian Association for the Cultivation of Science, Jadavpur, Calcutta 700 032, India, and Anorganische und Analytische Chemie der Universität Gesamthochschule Paderborn, D-33098 Paderborn, Germany

Received May 19, 1998

A number of mixed-ligand mononuclear and binuclear ruthenium(II) complexes of composition $[(bpy)_2Ru(H_3pzbzim)](ClO_4)_2\cdot 2H_2O$ (**1**), $[(phen)_2Ru(H_3pzbzim)](ClO_4)_2\cdot 3H_2O$ (**2**), $[(bpy)_2Ru(H_2pzbzim)Ru(bpy)_2](ClO_4)_3\cdot 5H_2O$ (**3**), $[(phen)_2Ru(H_2pzbzim)Ru(phen)_2](ClO_4)_3\cdot 4H_2O$ (**4**), $[(bpy)_2Ru(H_2pzbzim)Ru(phen)_2](ClO_4)_3\cdot 4H_2O$ (**5**), $[(bpy)_2Ru(pzbzim)Ru(bpy)_2](ClO_4)\cdot 3H_2O$ (**6**), and $[(phen)_2Ru(pzbzim)Ru(phen)_2](ClO_4)\cdot 2H_2O$ (**7**), where $H_3pzbzim$ = pyrazole-3,5-bis(benzimidazole), bpy = 2,2′-bipyridine, and phen = 1,10-phenanthroline, have been prepared and characterized. Complexes **3**−**5** isolated as mixtures of diastereoisomers have been separated by fractional recrystallization. In the cases of **3** and **4**, the *meso* (ΛΔ) and *racemate* (*rac*) (ΛΛ, ΔΔ) forms, and for **5**, two enantiomeric pairs [(ΛΔ, ΔΛ) and (ΛΛ, ΔΔ)] have been obtained. These, as well as the *meso* and *rac* diastereoisomers of **6**, have been characterized by ^1H and ^{13}C NMR spectroscopy. The crystal structure of the *meso* (ΛΔ) form of **3** ($C_{57}H_{53}N_{14}Cl_3O_{17}Ru_2$) has been determined, which crystallizes in the monoclinic space group $P2_1/c$ with $a = 11.672(2)$ Å, $b = 41.696(9)$ Å, $c = 12.871(2)$ Å, $\beta = 90.03(2)^o$, and $Z = 4$. The acid−base and redox chemistry of the binuclear complexes has been studied over the pH range 1−12 in acetonitrile−water (3:2) medium. The equilibrium constants of the species involving protonation and deprotonation of the benzimidazole NH protons and the metal oxidation states covering +2 and +3 have been evaluated by spectrophotometric and cyclic voltammetric measurements. During spectrophotometric titrations of the complexes with cerium(IV), the metal-to-ligand charge transfer transitions are replaced by the newly generated ligand-to-metal charge transfer transition. The luminescence spectra of the complexes in solution (at 298 K) and in frozen glass (at 77 K) and their quantum yields have been reported. In contrast to the luminescent behavior of **1**−**5**, corresponding deprotonated compounds do not fluoresce even at 77 K.

Introduction

Current intense interest in studying photochemical, photophysical, and electrochemical properties of bi- and polynuclear ruthenium(II) and osmium(II) complexes is stimulated by the goal to produce supramolecular multicomponent systems capable of functioning as photomolecular devices.[1−4] The extent of electronic communication between the metal centers in such complexes, mediated through the intervening bridging ligands, strongly influences their ground and excited state properties and redox activities.[5] The role of a bridging ligand in this context is determined by several factors, such as the arrangement and σ/π donor/acceptor properties of the coordination sites, the length and rigidity of spacers, the access of pathways for electron delocalization, and the charge of the ligand. If a bridging ligand can respond to an external perturbation like proton transfer, switching of properties in a complex species may take place.[6−8]

Over the past few years a number of neutral and anionic N-heterocyclic bridging ligands forming M−N−C−C−N chelate rings have been used to assemble ruthenium(II) or osmium(II) polypyridine building blocks.[1−5,9,10] The majority of these

* To whom correspondence should be addressed. E-mail: ickn@mahendra.iacs.res.in.

[†] Indian Association for the Cultivation of Science.

[‡] Universität Gesamthochschule Paderborn.

(1) Balzani, V.; Juris, A.; Venturi, M.; Campagna, S.; Serroni, S. *Chem. Rev.* **1996**, *96*, 759.
(2) Sauvage, J.-P.; Collin, J.-P.; Chambron, J.-C.; Guillerez, S.; Coudret, C.; Balzani, V.; Barigelletti, F.; De Cola, L.; Flamigni, L. *Chem. Rev.* **1994**, *94*, 993.
(3) Balzani, V., De Cola, L., Eds. *Supramolecular Chemistry*; Kluwer: Dordrecht, The Netherlands, 1992.
(4) Balzani, V.; Scandola, F. *Supramolecular Photochemistry*; Horwood: Chichester, U.K., 1991.
(5) Giuffrida, G.; Campagna, S. *Coord. Chem. Rev.* **1994**, *135/136*, 517.
(6) Haga, M.; Ali, M. M.; Maegawa, H.; Nozaki, K.; Yoshimura, A.; Ohno, T. *Coord. Chem. Rev.* **1994**, *94*, 99.
(7) Ward, M. D. *Chem. Soc. Rev.* **1995**, 121.
(8) Fabbrizzi, L.; Poggi, A. *Transition Metals in Supramolecular Chemistry;* Kluwer: Dordrecht, The Netherlands, 1994.
(9) Constable, E. C. *Prog. Inorg. Chem.* **1994**, *42*, 67.
(10) Harriman, A.; Ziessel, R. *Chem. Commun.* **1996**, 1707.
(11) (a) Hage, R.; Dijkhuis, A. H. J.; Haasnoot, J. G.; Prins, R.; Reedijk, J.; Buchanan, B. E.; Vos, J. G. *Inorg. Chem.* **1988**, *27*, 2185. (b) Barigelletti, F.; De Cola, L.; Balzani, V.; Hage, R.; Haasnoot, J. G.; Reedijk, J.; Vos, J. G. *Inorg. Chem.* **1989**, *28*, 4344. (c) Hage, R.; Haasnoot, J. G.; Nieuwenhuis, H. A.; Reedijk, J.; De Ridder, D. J. A.; Vos, J. G. *J. Am. Chem. Soc.* **1990**, *112*, 9245. (d) Hage, R.; Haasnoot, J. G.; Reedijk, J.; Wang, R.; Vos, J. G. *Inorg. Chem.* **1991**, *30*, 3263. (e) De Cola, L.; Barigelletti, F.; Balzani, V.; Hage, R.; Haasnoot, J. G.; Reedijk, J.; Vos, J. G. *Chem. Phys. Lett.* **1991**, *178*, 491. (f) Barigelletti, F.; De Cola, L.; Balzani, V.; Hage, R.; Haasnoot, J. G.; Reedijk, J.; Vos, J. G. *Inorg. Chem.* **1991**, *30*, 641. (g) van Diemen, J. H.; Hage, R.; Haasnoot, J. G.; Lempers, H. E. B.; Reedijk, J.; Vos, J. G.; De Cola, L.; Barigelletti, F.; Balzani, V. *Inorg. Chem.* **1992**, *31*, 3518. (h) Serroni, S.; Campagna, S.; Denti, G.; Keyes, T. E.; Vos, J. G. *Inorg. Chem.* **1996**, *35*, 4513.

10.1021/ic980564s CCC: $18.00
Published on Web 06/17/1999

bridging ligands are oligomeric pyridine/pyrazine/pyrimidine derivatives with appropriate symmetry and topology. They are usually electron-poor type ligands and mediate metal−metal interactions through low-lying π^* orbitals (LUMOs) by invoking electron transfer mechanisms. By contrast, electron-rich anionic bridging ligands, such as 3,5-bis(pyridin-2-yl)-1,2,4-triazolate(1−),[11] 3,5-bis(pyrazim-2-yl)-1,2,4-triazolate(1−),[11d,12] 2,2′-biimidazolate(2−),[13] and 2,2′-bibenzimidazolate(2−),[13,14] intercede intermetallic interactions via hole transfer mechanisms, taking advantage of relatively high lying filled molecular orbitals (HOMOs). Aside from these two types, there are some hybrid ligands which are electrically neutral but can be made anionic by deprotonating the constituent imidazole or triazole moieties after complex formation. Ruthenium(II) and osmium(II) complexes of this sort of ligand are of considerable interest because their redox, absorption, and emission properties can be subjected to fine-tuning by control of pH. Indeed, in a few cases proton-induced switching phenomena have been reported.[6,15] To this end, complexes of the bridging ligands 2,2′-bis(2-pyridyl)-bibenzimidazole,[6,16] 2,6-bis(2′-pyridyl)benzdiimidazole,[16b,17] 2,2′-bis(2-benzimidazolyl)-4,4′-bipyridine,[6,15] 1,3,5-tris[5-(pyridin-2-yl)-1,2,4-triazol-3-yl]benzene,[18] and 1,3,5-tris[5-(pyrazin-2-yl)-1,2,4-triazol-3-yl]benzene[18] in combination with 2,2′-bipyridine (bpy) or 1,10-phenanthroline (phen) have been studied extensively.

The present study is concerned with the synthesis, structural characterization, stereochemistry, redox activities, and spectroscopic properties of ruthenium complexes of a new bridging ligand 3,5-bis(benzimidazol-2-yl)pyrazole (H_3pzbzim) which

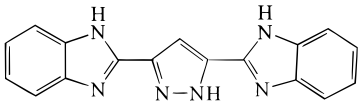

H_3pzbzim

forms the mononuclear complexes $[(L)_2Ru(H_3pzbzim)]^{2+}$ (L = bpy or phen) in the neutral form and the binuclear complexes $[(L)_2Ru(H_2pzbzim)Ru(L)_2]^{3+}$ in the monoanionic form after dissociation of the pyrazole NH proton. Since the binuclear complexes may exist, in principle, in two diastereoisomeric forms owing to the inherent chirality (Λ/Δ) of each of the metal centers, emphasis has been given toward separation of these stereoisomers and their characterization by ^{1}H and ^{13}C NMR spectroscopy. Moreover, as these complexes have dissociable imidazole NH protons, we have been interested in studying symbiotic proton and electron transfer reactions and evaluating the equilibrium constants involved therein.

Experimental Section

Materials. Reagent grade chemicals obtained from commercial sources were used as received. Solvents were purified and dried according to standard methods.[19] 3,5-Pyrazoledicarboxylic acid monohydrate,[20] $[Ru(bpy)_2Cl_2]\cdot 2H_2O$,[21] and $[Ru(phen)_2Cl_2]$[22] were prepared by the literature methods. $AgClO_4$ was prepared from "silver carbonate" and perchloric acid and recrystallized from benzene. The supporting electrolyte $[Et_4N](ClO_4)$[23] (TEAP) was prepared from $[Et_4N]Br$ and perchloric acid and recrystallized three times from hot water. The water used in electrochemical and spectrophotometric studies was deionized and distilled in an all-glass apparatus. The following buffer solutions[24] were used: $HClO_4-NaClO_4$, pH range 1−2; Robinson-Britton buffer, pH range 2−12.

Elemental (C, H, and N) analyses were performed in-house on a Perkin-Elmer 2400II analyzer.

Synthesis. Pyrazole-3,5-bis(benzimidazole) (H_3pzbzim). A mixture of *o*-phenylenediamine (5.4 g, 50 mmol) and 3,5-pyrazoledicarboxylic acid monohydrate (3.5 g, 20 mmol) and syrupy *o*-phosphoric acid (50 mL) was heated first at 200 °C for 2 h and then at 220 °C for another 2.5 h. The deep blue viscous solution was cooled to room temperature and poured into 1 L of crushed ice with vigorous stirring. A blue precipitate thus obtained was filtered off. It was slurried with water (ca. 500 mL) and slowly treated with 25% aqueous ammonia to pH ≈ 8 when the color changed to light pink. The solid was collected by filtration and washed several times with water. This was dissolved in a minimum quantity of hot (ca. 90 °C) *N*,*N*-dimethylformamide (DMF), stirred with a small amount of activated charcoal, and then filtered. To the filtrate was added water in small portions with stirring, and the product deposited as an off-white solid. This was recrystallized once again from a DMF−H_2O mixture: yield 3.6 g (60%); mp > 250 °C. Anal. Calcd for $C_{17}H_{12}N_6$: C, 67.99; H, 4.03; N, 27.90. Found: C, 67.69; H, 3.94; N, 27.74.

Complexes. All of the complexes were prepared under a nitrogen atmosphere. ***CAUTION*: $AgClO_4$ and the perchlorate salts of the metal complexes described below are potentially explosive and should be handled with great care!**

$[(bpy)_2Ru(H_3pzbzim)](ClO_4)_2\cdot 2H_2O$ (1). To a stirred suspension of *cis*-$[Ru(bpy)_2Cl_2]\cdot 2H_2O$ (0.52 g, 1 mmol) in ethanol (50 mL) was added solid $AgClO_4$ (0.42 g, 2 mmol). After 0.5 h, the precipitated AgCl was removed by filtration and the filtrate was treated with solid H_3pzbzim (0.36 g, 1.2 mmol) and 1 mL of 10^{-3} M $HClO_4$. The mixture was heated under reflux for 10 h with continuous stirring, after which it was filtered to remove the unreacted ligand. The filtrate on rotary evaporation gave the orange red crystalline product, which was collected by filtration. The compound was recrystallized from methanol−water (5:1) containing a few drops of 10^{-3} M $HClO_4$: yield 0.48 g (55%). Anal. Calcd for $C_{37}H_{32}N_{10}Cl_2O_{10}Ru$: C, 46.83; H, 3.16; N, 14.76. Found: C, 47.04, H, 3.23; N, 14.60.

$[(phen)_2Ru(H_3pzbzim)](ClO_4)_2\cdot 3H_2O$ (2). This compound was prepared in the same way as **1** using $[Ru(phen)_2Cl_2]$ as the starting complex: yield 0.6 g (60%). Anal. Calcd for $C_{41}H_{37}N_{10}Cl_2O_{11}Ru$: C, 48.52; H, 3.35; N, 13.80. Found: C, 48.34; H, 3.27; N, 13.68.

$[(bpy)_2Ru(H_2pzbzim)Ru(bpy)_2](ClO_4)_3\cdot 5H_2O$ (3). A solution of $[Ru(bpy)_2(EtOH)_2]^{2+}$ was prepared by stirring a mixture of $[Ru(bpy)_2Cl_2]0\cdot 2H_2O$ (0.52 g, 1 mmol) and $AgClO_4$ (0.42 g, 2 mmol) in ethanol (50 mL) for 0.5 h and removing the AgCl precipitated. To the

(12) Hughes, H. P.; Vos, J. G. *Inorg. Chem.* **1995**, *34*, 4001.
(13) Rillema, D. P.; Sahai, R.; Matthews, P.; Edwards, A. K.; Shaver, R. J.; Morgan, L. *Inorg. Chem.* **1990**, *29*, 167.
(14) (a) Haga, M. *Inorg. Chim. Acta* **1980**, *45*, L183. (b) Bond, A. M.; Haga, M. *Inorg. Chem.* **1986**, *25*, 4507. (c) Haga, M.; Matsumura-Inoue, T.; Yamabe, S. *Inorg. Chem.* **1987**, *26*, 4148. (d) Haga, M.; Bond, A. L. *Inorg. Chem.* **1991**, *30*, 475.
(15) Haga, M.; Ali, M. M.; Arakawa, R. *Angew. Chem., Int. Ed. Engl.* **1996**, *35*, 76.
(16) (a) Ohno, T.; Nozaki, K.; Haga, M. *Inorg. Chem.* **1992**, *31*, 548. (b) Nozaki, K.; Ohno, T.; Haga, M. *J. Phys. Chem.* **1992**, *96*, 10880. (c) Haga, M.; Ano, T.; Kano, K.; Yamabe, S. *Inorg. Chem.* **1991**, *30*, 3843. (d) Haga, M.; Ano, T.; Ishizaki, T.; Kano, K.; Nazaki, K.; Ohno, T. *J. Chem. Soc., Dalton Trans.* **1994**, 263.
(17) (a) Haga, M.; Ali, M. M.; Koseki, S.; Yoshimura, A.; Nozaki, K.; Ohno, T. *Inorg. Chim. Acta* **1994**, *226*, 17. (b) Ohno, T.; Nozaki, K.; Haga, M. *Inorg. Chem.* **1992**, *31*, 4256.
(18) (a) De Wolf, J. M.; Hage, R.; Haasnoot, J. G.; Reedijk, J.; Vos, J. G. *New J. Chem.* **1991**, *15*, 501. (b) Lempers, H. E. B.; Haasnoot, J. G.; Reedijk, J.; Hage, R.; Weldon, F. M.; Vos, J. G. *Inorg. Chim. Acta* **1994**, *225*, 67.
(19) Perrin, D. D.; Armarego, W. L.; Perrin, D. R. *Purification of Laboratory Chemicals*, 2nd ed.; Pergamon: Oxford, 1980.
(20) Lee, H. H.; Cain, B. F.; Denny, W. A.; Buckleton, J. S.; Clark, G. R. *J. Org. Chem.* **1989**, *54*, 428.
(21) Sullivan, B. P.; Meyer, T. J. *Inorg. Chem.* **1978**, *17*, 3334.
(22) Giordano, P. J.; Block, C. R.; Wrighton, M. S. *J. Am. Chem. Soc.* **1978**, *100*, 6960.
(23) Fry, A. J.; Britton, W. E. In *Laboratory Techniques in Electroanalytical Chemistry*; Kissinger, P. T., Heineman, W. R., Eds.; Marcel Dekker: New York, 1984.
(24) Perrin, D. D.; Dempsey, B. *Buffers for pH and Metal Ion Control*; Chapman and Hall: London, 1974.

filtrate were added H_3pzbzim (0.15 g, 0.5 mmol) and triethylamine (0.05 g, 0.5 mmol), and the solution was refluxed for 6 h, during which time the color changed from blood-red to orange-red. On cooling, the orange crystalline compound that deposited was collected by filtration: yield 0.45 g (60%). The proton NMR spectrum of the product indicated it to be a mixture of two diastereoisomers in the ratio 2:1. The *meso* ($\Lambda\Delta$) and *racemic* ($\Lambda\Lambda$, $\Delta\Delta$) forms were separated by fractional recrystallization from methanol. Of the two separated fractions **3a** and **3b**, the major fraction **3a** (*meso*) is relatively less soluble compared to **3b** (*racemate* (*rac*)). Anal. Calcd for $C_{57}H_{53}H_{14}Cl_3O_{17}Ru_2$: C, 45.16; H, 3.49; N, 12.94. Found for **3a**: C, 45.28; H, 3.29; N, 12.85. Found for **3b**: C, 45.42; H, 3.46; N, 13.02.

$[(phen)_2Ru(H_2pzbzim)Ru(phen)_2](ClO_4)_3\cdot 4H_2O$ (4). Starting from $[Ru(phen)_2Cl_2]$, the preparation of this compound was the same as described for **3**. The orange crystalline product thus obtained (65%) was again found from the ^{1}H NMR spectrum to be a mixture of two diastereoisomers in the ratio 3:2, the separation of which was achieved by successive recrystallization from a methanol−acetonitrile (2:1) mixture. The less souble, major fraction is designated as **4a** (*meso*) and the more soluble fraction as **4b** (*rac*). Anal. Calcd for $C_{65}H_{52}N_{14}Cl_3O_{16}Ru_2$: C, 49.01; H, 3.20; N, 12.31. Found for **4a**: C, 49.27; H, 3.10; N, 12.15. Found for **4b**: C, 48.86; H, 3.15; N, 12.24.

$[(bpy)_2Ru(H_2pzbzim)Ru(phen)_2](ClO_4)_3\cdot 4H_2O$ (5). To an ethanol solution (20 mL) of $[(phen)_2Ru(EtOH)_2]^{2+}$, generated from 0.27 g (0.5 mmol) of $[Ru(phen)_2Cl_2]$, were added a second ethanol solution (30 mL) of **1** (0.47 g, 0.5 mmol) and triethylamine (0.05 g, 0.5 mmol). The solution was refluxed for 6 h, after which it was allowed to evaporate slowly at room temperature. The crystalline product that deposited on standing overnight was filtered: yield 0.49 g (65%). This product was also found to be a mixture of two diastereoisomers in the ratio 3:2 and separated to **5a** (less soluble) and **5b** (more soluble) by fractional recrystallization from a methanol−acetonitrile (2:1) mixture. The diastereoisomers thus separated turn out to be two pairs of enantiomers; **5a** is the heterochiral ($\Lambda\Delta$, $\Delta\Delta$) enantiomeric pair and **5b** the *racemate* ($\Lambda\Lambda$, $\Delta\Delta$). Anal. Calcd for $C_{61}H_{51}N_{14}Cl_3O_{16}Ru_2$: C, 47.42; H, 3.30; N, 12.69. Found for **5a**: C, 47.47; H, 3.18; N, 12.51. Found for **5b**: C, 47.38; H, 3.19; N, 12.59.

$[(bpy)_2Ru(pzbzim)Ru(bpy)_2](ClO_4)\cdot 3H_2O$ (6). To a methanol solution (30 mL) of **3** (0.38 g, 0.25 mmol) was added a piece of freshly cut sodium metal (0.025 g, 1.1 mmol). The color of the solution changed immediately from red-orange to violet, and during stirring eventually a mauve microcrystalline compound deposited. The compound was filtered, washed with water, and dried in a vacuum. On recrystallization from acetonitrile violet crystals were obtained: yield 0.30 g (95%). Anal. Calcd for $C_{57}H_{47}N_{14}ClO_7Ru_2$: C, 53.58; H, 3.68; N, 15.35. Found: C, 53.67; H, 3.52; N, 15.45.

In this case, a clean separation of the two diastereoisomers could not be achieved by fractional recrystallization. However, starting from **3a** (*meso*) and **3b** (*rac*), the corresponding deprotonated diastereoisomers **6a** ($\Lambda\Delta$) and **6b** ($\Lambda\Lambda$, $\Delta\Delta$) were obtained in a pure state.

$[(phen)_2Ru(pzbzim)Ru(phen)_2](ClO_4)\cdot 2H_2O$ (7). Complex **4** (0.2 g, 0.125 mmol) dissolved in 20 mL of methanol on treatment with sodium (13 mg) gave a deep violet crystalline solid. The product obtained as a mixture of stereoisomers was recrystallized from methanol−acetonitrile (2:1): yield 0.16 g (90%). Anal. Calcd for $C_{65}H_{45}N_4ClO_6Ru_2$: C, 57.58; H, 3.32; N, 14.47. Found: C, 57.81; H, 3.41; N, 14.38.

Physical Measurements. Infrared spectra were recorded on a Perkin-Elmer 783 spectrophotometer using KBr disks. ^{1}H, ^{13}C, and $\{^1H-^1H\}$ COSY spectra were obtained on a Bruker Avance DPX 300 spectrometer using DMSO-d_6 solutions.

The electrochemical measurements were carried out with a BAS 100B electrochemistry system. A three-electrode assembly (BAS) comprising a Pt (for oxidation) or glassy carbon (for reduction) working electrode, Pt auxiliary electrode, and an aqueous Ag/AgCl reference electrode was used. The cyclic voltammetric (CV) and differential pulse voltammetric (DPV) measurements were carried out at 25 °C in acetonitrile solutions of the complexes (ca. 1 mM), and the concentration of the supporting electrolyte (TEAP) was maintained at 0.1 M. All of the potentials reported in this study were referenced against the Ag/AgCl electrode, which under the given experimental conditions gave a value of 0.36 V for the ferrocene/ferrocenium couple. The $E_{1/2}$ values were determined from CV using the relation $E_{1/2} = 0.5(E_{pc} + E_{pa})$, where E_{pc} and E_{pa} are cathodic and anodic potentials, respectively, while for DPV the relation used is $E_{1/2} = E_p + PA/2$, where E_p is the peak potential and PA stands for the pulse amplitude.

For the proton-coupled electrochemical measurements, 3:2 acetonitrile−water solutions of the complexes were employed because of the solubility limitation of the complexes in aqueous solution. The pH measurements were made with a Beckman Research Model pH meter in combination with a glass-calomel electrode assembly. As the pH meter responded reproducibly to hydrogen ion concentrations in the above solvent mixture, the "apparent" pH values obtained directly from the meter readings were referred to as pH. The $E_{1/2}$ value of the ferrocene/ferrocenium couple in acetonitrile−aqueous buffer (pH ≈ 7) medium was found to be 0.26 V vs Ag/AgCl.

Electronic absorption spectra were obtained with a Shimadzu UV 2100 spectrophotometer. The spectrophotometric titrations were carried out with a series of acetonitrile−water (3:2) solutions containing the same amount of the complex species ($\sim 10^{-5}$ M), and buffer solutions were added to adjust the pH in the range 1−12 (with an interval of about 0.4 pH unit), keeping the ratio of acetonitrile to water (3:2) fixed. The chemical oxidations of the diruthenium(II) complexes were followed spectrophotometrically by incremental addition of acidic solutions (HNO_3) of cerium(IV) ammonium nitrate in acetonitrile−water (3:2) to solutions of the complexes in the same solvent medium.

Emission spectra were recorded on an F-4500 Hitachi fluorescence spectrophotometer. The room temperature (298 K) spectra were obtained in either acetonitrile or methanol−ethanol (1:4) solutions using a 1 cm path length quartz cell. The spectra at 77 K were obtained in methanol−ethanol (1:4) glass by immersing a quartz finger dewar in liquid nitrogen. Quantum yields of the complexes (at 298 and 77 K) were determined in freeze−thaw−pump degassed methanol−ethanol (1:4) solutions of the complexes by a relative method using $[Ru(bpy)_3]^{2+}$ in the same solvent mixture as the standard.[25] The quantum yields were calculated using eq 1,[26]

$$\varphi_r = \varphi_{std}\frac{A_{std}}{A_r}\frac{I_r}{I_{std}}\frac{\eta_r^2}{\eta_{std}^2} \quad (1)$$

where φ_r and φ_{std} are the quantum yields of unknown and standard samples ($\varphi_{std} = 0.089$[27a] (at 298 K) and 0.35[27b] (at 77 K) in methanol−ethanol (1:4) at $\lambda_{ex} = 450$ nm), A_r and A_{std} (<0.1) are the solution absorbances at the excitation wavelength (λ_{ex}), I_r and I_{std} are the integrated emission intensities, and η_r and η_{std} are the refractive indices of the solvent. Experimental errors in the reported luminescence quantum yields were about 20%.

Crystal Structure Determination of $[(bpy)_2Ru(H_2pzbzim)Ru(bpy)_2](ClO_4)_3\cdot 5H_2O$ (3a). Crystals suitable for structure determination were obtained by slow evaporation of the methanol solution of the fraction **3a**.

Diffraction data were collected on a Siemens R3m/V diffractometer in the $\omega-2\theta$ scan mode using graphite-monochromatized Mo Kα radiation. Pertinent crystallographic data are summarized in Table 1. Three standard reflections were periodically monitored, which showed a decrease of about 7% intensity during data collection. The intensity data were corrected for Lorentz and polarization effects, and a semiempirical absorption correction was made from Ψ scans. A total of 15 044 reflections were collected in the range $\theta = 2.28-27.56°$, with $h = -15$ to 15, $k = 0$ to 54, and $l = 0$ to 16, of which 14 437 independent reflections ($R_{int} = 0.0566$) were used for structure determination. The structure was solved by direct and Fourier methods and refined by full-matrix least squares based on F^2 using the programs

(25) Sullivan, B. P.; Salmon, D. J.; Meyer, T. J.; Peedrin, J. *Inorg. Chem.* **1979**, *18*, 3369.
(26) van Houten, J.; Watts, R. J. *J. Am. Chem. Soc.* **1976**, *98*, 4853.
(27) (a) Cook, M. J.; Lewis, A. P.; McAuliffe, G. S. G.; Sharda, V.; Thomson, A. J.; Glasper, J. L.; Robbins, D. J. *J. Chem. Soc., Perkin Trans. 2* **1984**, 1293. (b) Crosby, G. A.; Elfring, W. H., Jr. *J. Phys. Chem.* **1976**, *80*, 2206.

Table 1. Crystallographic Data for the *meso* (ΛΔ) Form of $[(bpy)_2Ru(H_2pzbzim)Ru(bpy)_2](ClO_4)_3 \cdot 5H_2O$ (**3a**)

formula	$C_{57}H_{53}N_{14}Cl_{13}O_{17}Ru_2$	Z	4
fw	1514.62	λ(Mo Kα)	0.710 73
space group	$P2_1/c$	μ, mm^{-1}	0.691
a, Å	11.676(2)	ρ_{calcd}, g cm^{-3}	1.606
b, Å	41.696(9)	T, °C	20
c, Å	12.871(2)	R1,[a] ($I > 2\sigma(I)$)	0.0979
β, deg	90.03(2)	wR2[b] (all data)	0.4138
V, Å^3	6266(2)		

[a] $R1 = [\sum||F_o| - |F_c||/\sum|F_o|]$. [b] $wR2 = [\sum w(F_o^2 - F_o^2)^2/\sum(F_o)^2]^{1/2}$.

Scheme 1

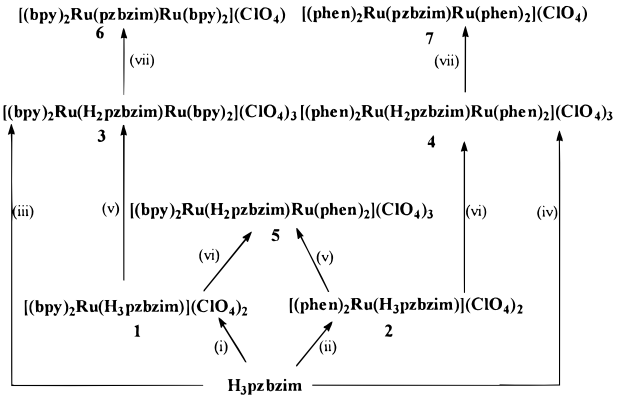

(i) $[Ru(bpy)_2Cl_2]$ (1 equiv)/$AgClO_4$ / $HClO_4$;
(ii) $[Ru(phen)_2Cl_2]$ (1 equiv)/$AgClO_4$ /$HClO_4$;
(iii) $[Ru(bpy)_2Cl_2]$(2 equiv) / $AgClO_4$ / Et_3N;
(iv) $[Ru(phen)_2Cl_2]$ (2 equiv)/$AgClO_4$ /Et_3N;
(v) $[Ru(bpy)_2Cl_2]$(1 equiv)/ $AgClO_4$ /Et_3N;
(vi) $[Ru(phen)_2Cl_2]$(1 equiv) /$AgClO_4$/ Et_3N;
(vii) NaOMe

SHELXTL-PLUS[28] and SHELXL-93.[29] Neutral atom scattering factors and anomalous dispersion terms were taken from Cromer and Waber.[30] The non-hydrogen atoms were refined anisotropically, while the hydrogen atoms were placed at the geometrically calculated positions with fixed isotropic thermal parameters. Of the three perchlorate ions, two (groups 2 and 3) were severely disordered, for which the chlorine sites were treated with a split model. Additionally, the electron density residuals for the solvent water molecules Wa4 and Wa5 were rather diffuse. Owing to these problems the final least-squares refinement ($I > 2.00\sigma(I)$) converged to rather high R values, R1 = 0.098 and wR2 = 0.263. The goodness of fit was 1.014, and the maximum and minimum peaks on the final difference Fourier map corresponded to 1.061 and −1.687 e Å^{-3}, respectively.

Results and Discussion

Synthesis. An outline of the syntheses of complexes **1**−**7** is given in Scheme 1. In terms of reaction time and yield the solvated cation $[L_2Ru(EtOH)_2]^{2+}$ (L = bpy or phen), generated by reacting stoichiometric amounts of *cis*-$[L_2RuCl_2]$ and $AgClO_4$, acts as a better precursor relative to *cis*-$[L_2RuCl_2]$ itself. To produce the mononuclear complexes $[L_2Ru(H_3pzbzim)](ClO_4)_2.nH_2O$ (**1**, **2**) free from corresponding pyrazole-deprotonated species, $[L_2Ru(H_2pzbzim)](ClO_4)$, it is necessary to carry out the reaction between $[L_2Ru(EtOH)_2]^{2+}$ and $H_3pzbzim$ under mildly acidic conditions. The "symmetrical" binuclear complexes $[L_2Ru(H_2pzbzim)RuL_2](ClO_4)_3 \cdot nH_2O$ (**3**, **4**) are readily obtained by reacting the appropriate $[L_2Ru(EtOH)_2]^{2+}$ species with the bridging ligand and triethylamine in the ratio 2:1:1, while the unsymmetrical diruthenium(II) compound $[(bpy)_2Ru(H_2pzbzim)Ru(phen)_2](ClO_4)_3 \cdot 4H_2O$ (**5**) can be produced by reacting either **1** with $[(phen)_2Ru(EtOH)_2]^{2+}$ or **2** with $[(bpy)_2Ru(EtOH)_2]^{2+}$. When complexes **3** and **4** are treated with a strong base such as sodium methoxide, they are quantitatively converted to the corresponding benzimidazole-deprotonated compounds $[L_2Ru(pzbzim)RuL_2](ClO_4) \cdot nH_2O$ (**6**, **7**).

Scheme 2

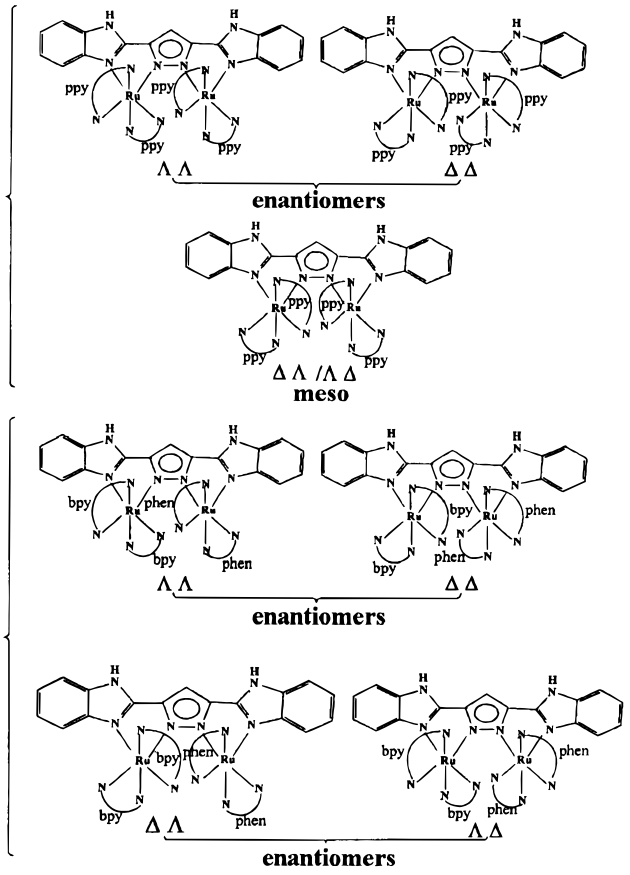

Isomerism. Inasmuch as the tris-diimine coordination sites for each of the metal centers in the binuclear complexes possess an element of chirality (Λ/Δ), the two centers, therefore, are either homochiral (ΛΛ or ΔΔ) or heterochiral (ΛΔ).[31] Consequently, as shown in Scheme 2, the binuclear complexes with the same terminal ligands (**3**, **4**, **6**, and **7**) can have two diastereoisomers, one a homochiral *rac* (ΛΛ, ΔΔ) and the other a heterochiral *meso* (ΛΔ) form. On the other hand, in the case of $[(bpy)_2Ru(H_2pzbzim)Ru(phen)_2](ClO_4)_3 \cdot 4H_2O$ (**5**), where the two chiral centers are not identical, there cannot be a *meso* form; the two diastereoisomers should be two enantiomeric pairs [(ΛΔ, ΔΛ) and (ΛΛ, ΔΔ)].

In the present study all the binuclear complexes initially isolated as mixtures of two diastereoisomers were separated by fractional recrystallization, advantage being taken of small differences in their solubility characteristics. In the case of **3**

(28) *SHELXTL-PLUS*; Siemens Crystallographic Research Systems: Madison, WI, 1990.
(29) Sheldrick, G. M. *SHELXL-93: A Program for Crystal Structure Refinement*. University of Göttingen: Göttingen, Germany, 1993.
(30) Cromer, D. T.; Waber, J. T. *International Tables for X-ray Crystallography*; The Kynoch Press: Birmingham, England, 1974; Vol. IV.
(31) (a) Keene, F. R. *Chem. Soc. Rev.* **1998**, *27*, 185. (b) von Zelewsky, A. *Stereochemistry of Coordination Compounds*; Wiley: Chichester, U.K., 1995. (c) Kelso, L. S.; Reitsma, D. A.; Keene, F. R. *Inorg. Chem.* **1996**, *35*, 5144.

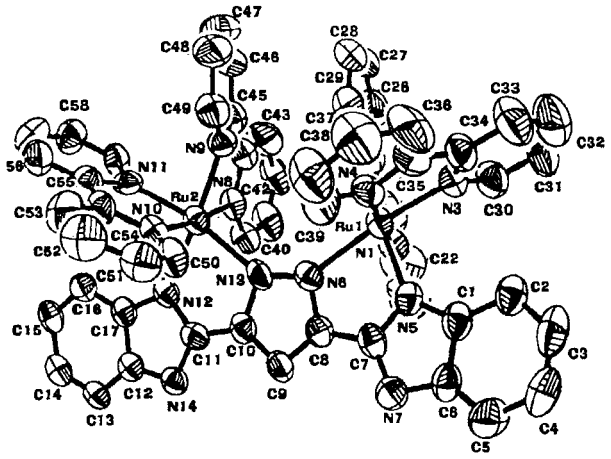

Figure 1. ORTEP representation of the structure of the $[(bpy)_2Ru(H_2pzbzim)Ru(bpy)_2]^{3+}$ cation in **3a** ($\Lambda\Delta$ *meso* form) showing the 50% probability of thermal ellipsoids.

methanol was used as the solvent, whereas for **4** and **5** a methanol−acetonitrile (2:1) mixture turned out to be more appropriate. Since a clean separation of the two diastereoisomers of **6** could not be effected by fractional crystallization, they were obtained by deprotonating the corresponding diastereoisomers of **3**. The less soluble diastereoisomers are referred to as **3a**, **4a**, **5a**, and **6a**, while the corresponding more soluble versions are **3b**−**6b**.

It is relevant to mention that the ratio of the proportions of the diastereoisomers in complexes **3**−**5**, as estimated by ^{1}H NMR integration, varies from 2:1 (for **3a**:**3b**) to 3:2 (for **4a**:**4b** and **5a**:**5b**), showing preferential occurrence of the less soluble diastereoisomer. Normally, statistical distribution of *meso* and *rac* forms should be expected and indeed has been reported[31a] for similar cases where quantification of the diastereoisomers could be made, with one notable exception[31c] showing greater abundance of the *meso* form relative to the *rac*. In the present context it appears that at the stage of isolation a part of the more soluble diastereoisomer remained unrecovered.

As will be seen, the crystal structure of the less soluble diastereoisomer **3a** conforms to the heterochiral *meso* ($\Lambda\Delta$) form, implying the more soluble **3b** to be the *rac* ($\Lambda\Lambda$, $\Delta\Delta$). By analogy, **4a** and **4b** should be the *meso* ($\Lambda\Delta$) and *rac* ($\Lambda\Lambda$, $\Delta\Delta$), respectively. It is also reasonable to assume that the more soluble **5b** is the *rac* ($\Lambda\Lambda$, $\Delta\Delta$), while the less soluble **5a** is the heterochiral enantiomeric pair ($\Lambda\Delta$ and $\Delta\Lambda$).

Description of the Crystal Structure of $[(bpy)_2Ru(H_2pzbzim)Ru(bpy)_2](ClO_4)_3\cdot 5H_2O$ (3a). An ORTEP representation of the cation in **3a** along with the atom labels is shown in Figure 1. Atomic coordinates and selected bond distances and angles are given in Tables2 and 3, respectively. The structure consists of two hexacoordinated ruthenium(II) centers in which the two $Ru(bpy)_2$ units are bridged by the pyrazolate nitrogens N(6) and N(3) of H_2pzbzim(−1) and the benzimidazole nitrogens N(5) and N(12) occupy the sixth coordination site. The basal planes of the two distorted RuN_6 octahedra are provided by the donor atoms of the bridging ligand and one nitrogen atom of each of the bpy ligands. In the case of Ru(1), the equatorial plane is best described by N(2), N(3), N(5), and N(6) atoms, the axial positions of which are occupied by N(4) and N(1) atoms, lying above and below this plane; Ru(1) lies below the mean plane by 0.022(1) Å. For Ru(2), the mean plane is formed by N(9), N(11), N(12), and N(13) atoms and the trans-axial N(10) and N(8) atoms placed above and below the metal plane complete the octahedron; the displacement of Ru(2) from the least-squares plane is only 0.007(1) Å. The stereochemical configurations at the two metal sites show some differences due to the different distortions present. The angle between the two vectors defined by Ru(1) and the midpoint of C(7) and C(8) on the one hand and by Ru(2) and the midpoint of C(10) and C(11) on the other is 23°. The deviations of the metal centers from idealized octahedral geometry are reflected in their bond angles: the cis angles vary from 77.4(3)° to 106.1(3)° for Ru(1) and 78.3(3)° to 108.1(3)° for Ru(2), while the trans angles vary between 170.8(4)° and 174.7(3)° for Ru(1) and 168.2(3)° and 174.7(3)° for Ru(2). The Ru−N bond distances lie in the range 2.016(9)−2.163(8) Å, of which Ru−N(pyrazolate) distances [Ru(1)−N(6) = 2.163(8) Å, Ru(2)−N(13) = 2.135(9) Å] are long, Ru−N(benzimidazole) distances [Ru(1)−N(5) = 2.105(9) Å, Ru(2)−N(12) = 2.079(8) Å] are intermediate, and Ru−N(bpy) distances [2.016(9)−2.068(9) Å] are short. The shortest metal−nitrogen bond lengths [Ru(1)−N(3) = 2.035(9) Å, Ru(2)−N(11) = 2.016(9) Å] are those in which the pyridine ring nitrogens are trans to the pyrazolate anion and are consistent with the improved Ru(dπ)−bpy(π*) back-bonding consequent to augmentation of electron density at the metal centers due to the strong σ-donor effect of the pyrazolate anion. The bite angles of the chelating ligands [bpy and H_2pzbzim(−1)] vary between 77.4° and 79.6°. The separation between the nonbonding Ru(1) and Ru(2) centers is 4.717(3) Å.

The crystal structure of **3a** (Figure 1) clearly shows that the two ruthenium centers in this diastereoisomer are heterochiral. Using the notion of chirality descriptors,[31b] Ru(1) and Ru(2) sites can be labeled as Δ and Λ, respectively. Accordingly, the less soluble diastereoisomer **3a** is the *meso* ($\Lambda\Delta$) form.

NMR Spectra. The ^{1}H, {^{1}H−^{1}H} COSY, and ^{13}C NMR spectra for complexes **3**−**7** have been recorded in $(CD_3)_2SO$ solutions at room temperature. The numbering schemes used to interpret these spectra are given in Chart 1.

$[(bpy)_2Ru(H_2pzbzim)Ru(bpy)_2](ClO_4)_3\cdot 5H_2O$ (3a, 3b). The ^{1}H NMR spectrum of **3**, as isolated, showed the presence of a number of overlapping signals, including two closely spaced doublets at 5.04 and 5.06 ppm and two singlets at 14.38 and 14.46 ppm. Since the ratio of the integrated areas of the two doublets as well as of the two singlets was found to be 2:1, it was clear at the outset that **3** is composed of two diastereoisomers in the above-mentioned ratio. As mentioned, the separation of the diastereoisomeric pair was achieved by successive recrystallization from methanol. The less soluble, major fraction (**3a**) exhibits the doublet at 5.04 ppm and the singlet at 14.38 ppm, while for the more soluble fraction (**3b**) these signals are observed at 5.06 and 14.46 ppm. As it has already been noted, the crystal structure of **3a** conforms to the *meso* ($\Lambda\Delta$) form and by implication **3b** is the *rac* ($\Lambda\Lambda$, $\Delta\Delta$). The ^{1}H NMR spectra of **3a** and **3b** are shown in Figure 2, and the chemical shifts are listed in Table 4.

For **3a** ($\Lambda\Delta$), the CH resonances due to the bridging ligand are observed between 5.04 and 8.12 ppm and those due to the bipyridines between 6.39 and 8.47 ppm. On the other hand, the corresponding ranges for **3b** ($\Lambda\Lambda$, $\Delta\Delta$) are 5.06−8.05 and 6.72−8.59 ppm. The benzimidazole NH proton is profoundly downfield shifted in the diastereoisomers **3a** (14.38 ppm) and **3b** (14.46 ppm) due to H-bonding with $(CD_3)_2SO$. The highest field resonances in **3a** (5.04 ppm) and **3b** (5.06 ppm) are attributable to H(14), because this proton experiences maximum shielding due to the anisotropic ring current effect of the adjacent bipyridine rings.[32] The assignments of the other resonances have

(32) Orellana, G.; Ibarra, C. A.; Santoro, J. *Inorg. Chem.* **1988**, *27*, 1025.

Table 2. Atomic Coordinates ($\times 10^4$) and Equivalent Isotropic Displacement Parameters ($Å^2 \times 10^3$) for the *meso* ($\Lambda\Delta$) Form of $[(bpy)_2Ru(H_2Pzbzim)Ru(bpy)_2](ClO_4)_3 \cdot 5H_2O$ (**3a**)

atom	*x*	*y*	*z*	*U*(eq)[a]	atom	*x*	*y*	*z*	*U*(eq)[a]
Ru(1)	−2162(1)	3420(1)	6565(1)	54(1)	C(35)	−1584(12)	2763(3)	7122(11)	77(4)
Ru(2)	675(1)	4186(1)	7369(1)	46(1)	C(36)	−1122(17)	2505(3)	7638(14)	110(6)
N(1)	−2863(9)	3748(2)	5542(7)	61(2)	C(37)	−465(17)	2584(5)	8515(15)	117(6)
N(2)	−905(8)	3432(2)	5444(7)	62(2)	C(38)	−335(16)	2881(5)	8880(13)	112(6)
N(3)	−2666(8)	3018(2)	5778(7)	63(2)	C(39)	−828(13)	3119(4)	8316(12)	98(5)
N(4)	−1417(8)	3073(2)	7448(8)	63(2)	C(40)	−422(11)	4557(3)	5600(9)	63(3)
N(5)	−3557(7)	3403(2)	7598(7)	55(2)	C(41)	−596(13)	4634(3)	4549(10)	84(4)
N(6)	−1831(7)	3823(2)	7580(6)	48(2)	C(42)	15(14)	4488(4)	3824(10)	85(4)
N(7)	−4479(8)	3624(2)	8935(7)	64(2)	C(43)	782(14)	4238(4)	4095(10)	88(4)
N(8)	312(7)	4327(2)	6874(6)	51(2)	C(44)	893(10)	4165(3)	5125(8)	57(3)
N(9)	1386(7)	3814(2)	6534(7)	55(2)	C(45)	1610(10)	3894(3)	5511(8)	60(3)
N(10)	1164(7)	4025(2)	8802(6)	48(2)	C(46)	2451(11)	3740(4)	4942(11)	80(4)
N(11)	2318(7)	4334(2)	7411(7)	55(2)	C(47)	3022(13)	3485(4)	5404(15)	98(5)
N(12)	99(7)	4606(2)	8071(6)	50(2)	C(48)	2772(13)	3395(4)	6359(14)	93(5)
N(13)	−1089(7)	4079(2)	7627(6)	51(2)	C(49)	1956(11)	3568(3)	6932(10)	67(3)
N(14)	−1309(7)	4872(2)	8842(6)	50(2)	C(50)	533(11)	3853(3)	9493(8)	64(3)
C(1)	−4457(10)	3198(3)	7874(10)	63(3)	C(51)	935(13)	3739(3)	10402(9)	77(4)
C(2)	−4844(11)	2906(3)	7450(11)	71(3)	C(52)	2032(15)	3810(4)	10689(11)	97(5)
C(3)	−5762(12)	2768(4)	7924(14)	94(5)	C(53)	2703(13)	3994(4)	10030(11)	95(5)
C(4)	−6302(13)	2894(4)	8759(14)	95(5)	C(54)	2288(10)	4093(3)	9069(8)	58(3)
C(5)	−5959(12)	3183(4)	9165(12)	89(4)	C(55)	2920(10)	4274(3)	8289(9)	62(3)
C(6)	−5045(10)	3336(3)	8726(9)	61(3)	C(56)	4057(12)	4371(3)	8431(11)	80(4)
C(7)	−3584(10)	3643(3)	8255(8)	55(3)	C(57)	4568(11)	4533(4)	7641(13)	88(4)
C(8)	−2730(9)	3898(3)	8206(8)	51(2)	C(58)	4010(11)	4599(4)	6743(11)	78(4)
C(9)	−2645(9)	4187(3)	8656(8)	56(3)	C(59)	2898(10)	4495(3)	6670(8)	62(3)
C(10)	−1599(9)	4304(2)	8253(8)	50(2)	Cl(1)	7652(6)	1557(1)	6253(5)	155(3)
C(11)	−974(9)	4595(3)	8412(7)	51(2)	O(11)	7788(14)	1223(4)	6346(13)	186(7)
C(12)	−431(9)	5084(2)	8768(7)	49(2)	O(12)	6978(21)	1679(6)	7149(18)	324(16)
C(13)	−298(10)	5402(2)	9089(8)	53(2)	O(13)	8788(17)	1705(5)	6399(18)	267(11)
C(14)	708(11)	5542(3)	8946(9)	64(3)	O(14)	7125(19)	1667(6)	5340(16)	272(12)
C(15)	1653(11)	5381(3)	8480(8)	58(3)	Cl(21)	1793(8)	2255(3)	6511(8)	72(5)
C(16)	1536(9)	5064(3)	8169(8)	58(3)	Cl(22)	2481(31)	2089(9)	6420(23)	363(14)
C(17)	489(9)	4918(3)	8310(7)	51(2)	O(21)	1901(24)	2266(7)	7498(24)	274(11)
C(20)	−3796(12)	3917(3)	5677(10)	78(4)	O(22)	3453(61)	1843(18)	7470(53)	566(37)
C(21)	−4142(15)	4151(4)	4955(14)	103(5)	O(23)	932(41)	2031(12)	6278(31)	400(21)
C(22)	−3554(18)	4199(4)	4095(13)	113(6)	O(24)	1728(31)	2494(9)	6079(27)	327(15)
C(23)	−2533(16)	4026(4)	3927(11)	100(5)	Cl(31)	3331(7)	292(3)	8409(7)	88(3)
C(24)	−2228(11)	3800(3)	4683(10)	71(3)	Cl(32)	3313(15)	149(6)	8721(16)	144(6)
C(25)	−1177(12)	3604(3)	4557(10)	74(4)	O(31)	4515(17)	239(5)	8280(15)	196(7)
C(26)	−542(14)	3553(4)	3648(10)	88(4)	O(32)	3339(25)	551(8)	9075(23)	285(12)
C(27)	309(15)	3347(4)	3632(14)	98(5)	O(33)	2587(32)	138(10)	9337(29)	352(18)
C(28)	616(13)	3183(4)	4471(13)	90(4)	O(34)	2780(22)	398(7)	7572(21)	147(11)
C(29)	−16(11)	3227(3)	5417(11)	75(3)	O(35)	2799(34)	−44(10)	8013(31)	167(17)
C(30)	−3330(12)	3014(4)	4928(11)	86(4)	WA1	5618(11)	977(4)	5882(9)	126(4)
C(31)	−3683(16)	2730(5)	4449(15)	112(6)	WA2	−3483(10)	4995(4)	9679(9)	143(6)
C(32)	−3260(19)	2444(6)	4843(15)	128(7)	WA3	4719(12)	5322(4)	8730(13)	169(6)
C(33)	−2613(16)	2446(4)	5696(16)	116(6)	WA4	4083(22)	1061(7)	7452(21)	278(12)
C(34)	−2288(11)	2734(3)	6173(11)	73(3)	WA5	4560(33)	1696(9)	7879(28)	324(15)

[a] *U*(eq) is defined as one-third of the trace of the orthogonalized $\mathbf{U}_{ij}$ tensor.

been made with the help of the $\{^1H-^1H\}$ COSY spectra (that of **3a** is shown in Figure 3). In **3a** ($\Lambda\Delta$), the triplet observed at 6.76 ppm with its cross peak at 5.04 ppm is assignable to H(13). Similarly, the multiplet at 7.18 ppm can be attributed to H(12) since it is correlated to H(13) and H(11); the resonance due to H(11) occurs as a doublet at 7.63 ppm. The singlet due to the H(7) proton of the central pyrazolate ring, which shows no cross peak, is considerably shifted to a lower field (8.12 ppm) relative to that of the free ligand (7.43 ppm) and signifies the strong σ-donor property of the pyrazolate bridge. As expected, the resonances observed for the bridging ligand in **3b** ($\Lambda\Lambda$, $\Delta\Delta$) are similar to those of **3a** ($\Lambda\Delta$), but not identical.

The assignments of the resonances due to the bipyridines in the two diastereoisomers were further aided by the following facts. Usually for $Ru(bpy)_n^{2+}$ species, the decreased order of chemical shifts is H(3) > H(4) ≥ H(5) > H(6). The protons H(3) and H(6) are normally observed as doublets, while H(4) and H(5) appear either as triplet or doublet of doublet. The spin coupling constants are $J_{3,4}$ and $J_{4,5} \approx 8$ Hz, $J_{5,6} \approx 5$ Hz, and $J_{3,5}$ and $J_{4,6} \approx 1.2$ Hz.[33−38] These, along with the COSY spectra, have enabled us to identify spin−spin interactions in each of the four pairs of pyridine rings (designated as A, B, C, D) in **3a** and **3b** (Table 4).

The ^{13}C NMR spectra of both **3a** (*meso*) and **3b** (*rac*) exhibit 29 lines in the range 104−159 ppm (Table 5), of which 20 lines

(33) Constable, E. C.; Seddon, K. R. *J. Chem. Soc., Chem. Commun.* **1982**, 34.
(34) Walsch, J. L.; Durham, B. *Inorg. Chem.* **1982**, *21*, 329.
(35) Steel, P. J.; Lahousse, F.; Lerner, D.; Marzin, C. *Inorg. Chem.* **1983**, *22*, 1488.
(36) (a) Hage, R.; Prins, R.; Haasnoot, J. G.; Reedijk, J.; Vos, J. G. *J. Chem. Soc, Dalton Trans.* **1987**, 1389. (b) Hage, R.; Haasnoot, J. G.; Reedijk, J.; Vos, J. G. *Inorg. Chim. Acta* **1986**, *118*, 73.
(37) Bolger, J.; Gourdon, A.; Ishow, E.; Launay, J.-P. *Inorg. Chem.* **1996**, *35*, 2937.
(38) Kelso, L. S.; Reitsma, D. A.; Keene, F. R. *Inorg. Chem.* **1996**, *35*, 5144.

Table 3. Selected Bond Distances (Å) and Angles (deg) for the *meso* (ΛΔ) Form of $[(bpy)_2Ru(H_2pzbzim)Ru(bpy)_2](ClO_4)_3 \cdot 5H_2O$ (**3a**)

Ru(1)−N(1)	2.068(9)	Ru(2)−N(8)	2.056(7)
Ru(1)−N(2)	2.059(10)	Ru(2)−N(9)	2.063(9)
Ru(1)−N(3)	2.045(9)	Ru(2)−N(10)	2.045(8)
Ru(1)−N(4)	2.035(9)	Ru(2)−N(11)	2.016(9)
Ru(1)−N(5)	2.105(9)	Ru(2)−N(12)	2.079(9)
Ru(1)−N(6)	2.163(8)	Ru(2)−N(13)	2.135(9)
Ru(1)···Ru(2)	4.717(3)		
N(1)−Ru(1)−N(2)	79.6(4)	N(8)−Ru(2)−N(9)	79.0(4)
N(1)−Ru(1)−N(3)	96.5(4)	N(8)−Ru(2)−N(10)	174.7(3)
N(1)−Ru(1)−N(4)	174.4(4)	N(8)−Ru(2)−N(11)	97.6(3)
N(1)−Ru(1)−N(5)	96.8(4)	N(8)−Ru(2)−N(12)	95.7(3)
N(1)−Ru(1)−N(6)	86.6(3)	N(8)−Ru(2)−N(13)	90.4(3)
N(2)−Ru(1)−N(3)	83.0(4)	N(9)−Ru(2)−N(10)	96.3(3)
N(2)−Ru(1)−N(4)	96.0(4)	N(9)−Ru(2)−N(11)	82.0(4)
N(2)−Ru(1)−N(5)	174.7(3)	N(9)−Ru(2)−N(12)	171.6(3)
N(2)−Ru(1)−N(6)	106.1(3)	N(9)−Ru(2)−N(13)	108.1(3)
N(3)−Ru(1)−N(4)	79.4(4)	N(10)−Ru(2)−N(11)	79.1(4)
N(3)−Ru(1)−N(5)	93.6(4)	N(10)−Ru(2)−N(12)	88.6(3)
N(3)−Ru(1)−N(6)	170.8(4)	N(10)−Ru(2)−N(13)	93.4(3)
N(4)−Ru(1)−N(5)	87.4(4)	N(11)−Ru(2)−N(12)	92.3(3)
N(4)−Ru(1)−N(6)	98.0(3)	N(11)−Ru(2)−N(13)	168.2(3)
N(5)−Ru(1)−N(6)	77.4(3)	N(12)−Ru(2)−N(13)	78.3(3)

Chart 1

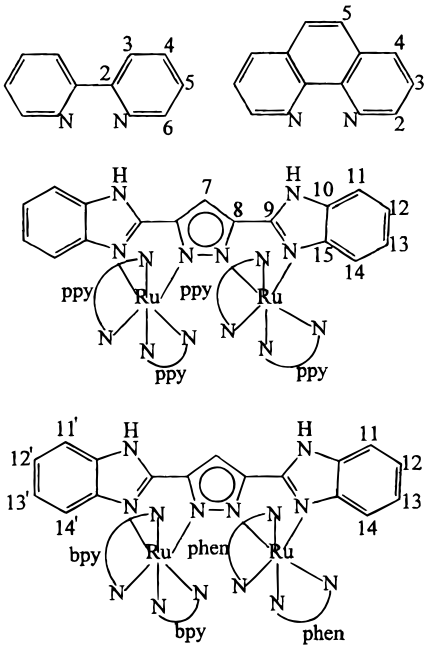

are attributable to the four pyridine rings and the remaining 9 lines to the bridging ligand.

$[(phen)_2Ru(H_2pzbzim)Ru(phen)_2](ClO_4)_3 \cdot 4H_2O$ (4a, 4b). As already stated, two diastereoisomers have been isolated for **4**. Before separation of these isomers, the ^{1}H NMR spectrum of **4** (Supporting Information) shows the presence of a large number of overlapping signals, but again similar to **3**, there are two closely spaced doublets at 4.63 and 4.71 ppm, the areas of which are in the ratio 3:2. Since H(14) is most shielded by the ring current effect of the contiguous *o*-phenanthroline, the occurrence of the two doublets provided a clear signature of the presence of two diastereoisomers in the ratio 3:2. These two diastereoisomers were separated by successive recrystallization from methanol−acetonitrile (2:1), and the less soluble fraction (**4a**) with the doublet at 4.63 ppm turned out to be the major isomer. By analogy to **3a** and **3b**, the less soluble diastereoisomer **4a** is regarded as the *meso* (ΛΔ) form and the more soluble fraction **4b** as the *racemic* (ΛΛ, ΔΔ) mixture. The ^{1}H NMR spectra of **4a** and **4b** are shown in Figure 4. The spectral assignments have been made, as before, from their COSY spectra (Supporting Information), and the results are given in Table 6. As expected, the chemical shifts due to the bridging ligand differ only to a small extent in the two isomers; however, the sequences of resonances for the *o*-phenanthrolines in the two cases are quite different.

The distinctive features of the two diastereoisomers are further reflected in their ^{13}C NMR spectra (Table 5). Both **4a** (*meso*)

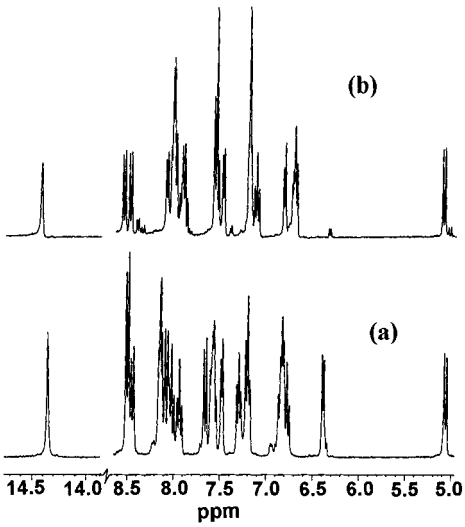

Figure 2. ^{1}H NMR spectra of the diastereoisomers **3a** (a) and **3b** (b) of the complex $[(bpy)_2Ru(H_2pzbzim)Ru(bpy)_2](ClO_4)_3 \cdot 5H_2O$ in $(CD_3)_2SO$: (a) *meso* (ΛΔ); (b) *rac* (ΛΛ, ΔΔ).

Table 4. ^{1}H NMR Data[a] for the Two Diastereoisomers *meso* (ΛΔ) **3a** and *rac* (ΛΛ, ΔΔ) **3b** of $[(bpy)_2Ru(H_2Pzbzim)Ru(bpy)_2](ClO_4)_3 \cdot 3H_2O$ (**3**) in $(CD_3)_2SO$

proton[b]	**3a** (ΛΔ)	**3b** (ΛΛ, ΔΔ)
	Bridging Ligand	
H(11)	7.63; 2H; 8.2	7.59, 2H, 8.1
H(12)	7.18; 2H; 7.6	7.13, 2H, 7.8
H(13)	6.76; 2H; 7.8	6.70, 2H, 7.8
H(14)	5.04; 2H; 8.3	5.06, 2H, 8.3
H(7)	8.12; 1H	8.05, 1H
NH	14.38, 2H	14.46, 2H
	bpy Ligands	
ring A		
H(3)	8.05; 2H; 8.3	8.02, 2H, 8.2
H(4)	7.55; 2H; 7.1	7.56, 2H, 7.8
H(5)	6.83; 2H; 7.1	6.72, 2H, 6.8
H(6)	6.39; 2H; 5.3	6.82, 2H, 5.3
ring B		
H(3)	8.42; 2H; 8.0	8.02, 2H, 8.2
H(4)	7.91; 2H; 7.8	7.56, 2H, 7.8
H(5)	7.18; 2H; 6.9	7.21, 2H, 6.8
H(6)	6.81; 2H; 5.6	7.20, 2H, 5.4
ring C		
H(3)	8.47; 2H; 8.0	8.52, 2H, 8.1
H(4)	8.00; 2H; 7.6	7.92, 2H, 7.8
H(5)	7.18; 2H; 6.9	7.21, 2H, 6.8
H(6)	7.47; 2H; 5.6	7.50, 2H, 5.5
ring D		
H(3)	8.47; 2H; 8.0	8.59, 2H, 8.1
H(4)	8.06; 2H; 7.8	8.07, 2H, 7.8
H(5)	8.13; 2H; 6.9	7.97, 2H, 6.8
H(6)	7.56; 2H; 5.5	8.12, 2H, 5.5

[a] For ^{1}H NMR data respectively: chemical shift (ppm), number of protons, *J* (Hz). H(3) and H(6) are doublets; H(4) and H(5) are triplets or doublets of doublets. [b] For atom numbering scheme see Chart 1.

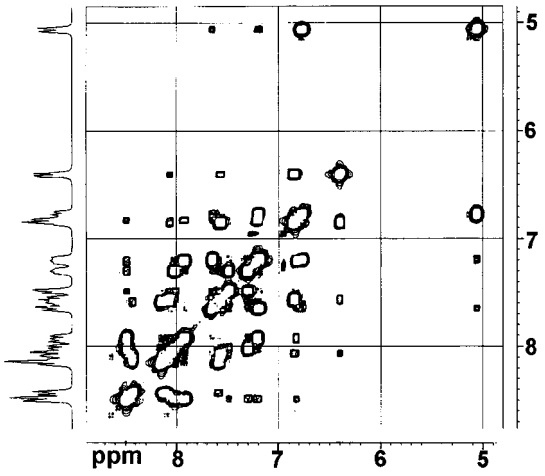

Figure 3. $\{^1H-^1H\}$ COSY NMR spectrum of the *meso* ($\Lambda\Delta$) diastereoisomer **3a** of the complex $[(bpy)Ru(H_2pzbzim)Ru(bpy)_2](ClO_4)_3\cdot 5H_2O$ in $(CD_3)_2SO$.

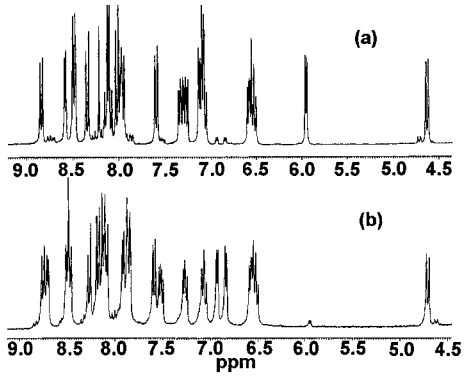

Figure 4. ^1H NMR spectra of the diastereoisomers **4a** (a) and **4b** (b) of the complex $[(phen)_2Ru(H_2pzbzim)Ru(phen)_2](ClO_4)_3\cdot 4H_2O$ in $(CD_3)_2SO$: (a) *meso* ($\Lambda\Delta$); (b) *rac* ($\Lambda\Lambda$, $\Delta\Delta$).

and **4b** (*rac*) exhibit 33 lines due to the four phenanthrolines (4 × 6 lines) and the bridging ligand (9 lines). The chemical shifts in the two cases for the same carbon atoms show small but significant differences.

$[(bpy)_2Ru(H_2pzbzim)Ru(phen)_2](ClO_4)_3\cdot 4H_2O$ (5a, 5b). The ^1H NMR spectrum of **5** also revealed the presence of two diastereoisomers (**5a** and **5b**), again in the ratio 3:2. However, compared to **3a** and **3b** or **4a** and **4b**, the spectra of **5a** and **5b** (Figure 5) exhibit a greater number of signals because here the two benzimidazole units of the bridging ligand are no longer magnetically equivalent. As already mentioned, the diastereoisomers **5a** and **5b** are two pairs of enantiomers [($\Lambda\Delta$, $\Delta\Lambda$) and ($\Lambda\Lambda$,$\Delta\Delta$)], of which the less soluble **5a** is composed of the heterochiral ($\Lambda\Delta$, $\Delta\Lambda$) enantiomeric pair. In the case of **5a** ($\Lambda\Delta$, $\Delta\Lambda$), the two most shielded doublets observed at 4.75 ppm (J = 8.2 Hz) and 5.02 ppm (J = 8.4 Hz) are due to H(14) connected to the $Ru(phen)_2$ fragment and H(14′) attached to the $Ru(bpy)_2$ fragment, respectively. On the other hand, for the *rac* **5b** ($\Lambda\Lambda$, $\Delta\Delta$), the doublets due to H(14) and H(14)′ are observed at 4.80 (J = 8.4 Hz) and 5.05 (J = 8.3 Hz), respectively. Table 7 summarizes the chemical shifts of **5a** and **5b**. The two enantiomeric pairs have been further characterized by their ^{13}C NMR spectra. As given in Table 5, both exhibit 36 resonances due to the bipyridines (2 × 5 lines), the phenanthrolines (2 × 6 lines), and the bridging ligand (14 lines).

$[(bpy)_2Ru(pzbzim)Ru(bpy)_2](ClO_4)\cdot 3H_2O$ (6a, 6b). The stereoisomers **6a** ($\Lambda\Delta$) and **6b** ($\Lambda\Lambda$, $\Delta\Delta$) have been obtained by the direct deprotonation of the *meso* ($\Lambda\Delta$) **3a** and the *rac* ($\Lambda\Lambda$, $\Delta\Delta$) **3b**, respectively. Their ^1H NMR spectra are shown in Figure 6, and the chemical shift values are collected in Table 8. It may be noted that the protons associated with the bridging ligand in **6a** (*meso*) and **6b** (*rac*) are all upfield shifted by 0.28−0.60 ppm relative to their precursors **3a** and **3b**. The pronounced shielding effect is a consequence of the increase in electron density of the benzimidazole moiety due to deprotonation. As expected, maximum shielding occurs for H(7), followed by H(12) and H(13). The assignments of the bipyridine protons have been made in the usual way from the COSY spectra. A comparison of the spectra of **6a** and **6b** vis-à-vis **3a** and **3b** reveals that no change in configuration of the diastereoisomers takes place on deprotonation.

Redox Properties. The redox activities of complexes **1**−**6** have been studied in acetonitrile solution, and the relevant electrochemical data are given in Table 9. Except for **6**, in all of the cases the metal-centered oxidations take place reversibly, as borne out by the facts that the peak-to-peak separation ($E_{pa} - E_{pc} = 65 \pm 5$ mV) and the ratio of the peak heights ($i_{pa}/i_{pc} \approx 1$) for the redox couples remain constant with the variation of scan rates (υ = 50−500 mV s^{-1}), and the current height shows a linear dependence on the square root of the scan rate. The cyclic voltammogram of **3** (Figure 7), which is typical of the binuclear systems, shows that the two metal centers get stepwisely oxidized at 1.01 and 1.23 V. For the deprotonated complex **6**, however, the oxidations at the metal sites take place quasi-reversibly with $E_{1/2}(1) = 0.63$ V and $E_{1/2}(2) = 0.96$ V. It may be noted that the redox potentials for the isomers **4a** (1.02 and 1.25 V) and **4b** (1.01 and 1.23 V) as well as **5a** (1.01 and 1.22 V) and **5b** (1.00 and 1.24 V) are not much different from those for **3a** and **3b**, indicating that in these series of compounds the electron transfer reactions at the metal centers are not much affected due to the variations of either the stereoisomers or the terminal polypyridine ligands.

As compared to the mononuclear cation [**1** or **2**]$^{2+}$, for which the oxidation of the ruthenium(II) center occurs at 0.90 V, the first metal center in the binuclear cation [**3**−**5**]$^{3+}$ is oxidized at a more positive potential (ca. 1.01 V). By contrast, the first metal center in the deprotonated binuclear cation [**6**]$^{+}$ undergoes oxidation at a much lower potential (0.63 V). Clearly, with the depletion of the cationic charge the metal center becomes more electron rich and more susceptible to oxidation. It is of interest to note that the equilibrium constant K_c for the comproportionation reaction, $Ru^{II}Ru^{II} + Ru^{III}Ru^{III} \rightleftharpoons 2Ru^{II}Ru^{III}$, as obtained from the separation of the two redox potentials ($\Delta E_{1/2} = E_{1/2}(2) - E_{1/2}(1)$) and using the relation $RT \ln K_c = nF\Delta E_{1/2}$, varies from 2×10^3 to 1×10^4 (at T = 298 K) for complexes **3**−**5**. By comparison, the value of K_c for **6** (4×10^5) is 1−2 orders of magnitude greater. This indicates that the mixed-valence state gets relatively more stabilized when the bridging ligand is fully deprotonated. The magnitude of K_c depends, inter alia, on the electrostatic and magnetic superexchange interactions and electron delocalization.[39,40] The effect of deprotonation in the present case seems to augment electron delocalization in the system. It may be noted that class II systems according to the Robin−Day classification[41] show an intermediate degree of delocalization with K_c typically lying in the range 10^2−10^6.

The electrochemical responses of **1**−**6** in the potential window 0 to −2.2 V are summarized in Table 9. The mononuclear complexes are found to undergo two successive one-electron reversible reductions. For the binuclear complexes three reduc-

(39) Richardson, D. E.; Taube, H. *Coord. Chem. Rev.* **1984**, *60*, 107.
(40) Crutchley, R. J. *Adv. Inorg. Chem.* **1994**, *41*, 273.
(41) Robin, M. B.; Day, P. *Adv. Inorg. Chem. Radiochem.* **1967**, *10*, 247.

Table 5. ^{13}C NMR Data for the Diastereoisomers **3a** ($\Lambda\Delta$) and **3b** ($\Lambda\Lambda$, $\Delta\Delta$), **4a** ($\Lambda\Delta$) and **4b** ($\Lambda\Lambda$, $\Delta\Delta$), and **5a** ($\Lambda\Delta$, $\Delta\Lambda$) and **5b** ($\Lambda\Lambda$, $\Delta\Delta$) in $(CD_3)_2SO$

3a	104.68, 113.25, 113.82, 122.84, 123.25, 123.34, 123.71, 123.97, 124.54, 127.87, 126.25, 127.15, 127.31, 127.50, 135.58, 136.44, 137.08, 137.68, 141.80, 147.29, 148.99, 150.16, 150.78, 151.59, 152.65, 156.40, 156.93, 157.14, 158.50
3b	106.10, 113.80, 113.89, 123.68, 124.16, 124.32, 124.42, 124.49, 125.29, 126.72, 127.60, 127.85, 127.96, 134.73, 136.11, 136.95, 137.63, 138.21, 141.81, 147.08, 149.44, 149.75, 151.22, 152.04, 153.10, 153.79, 157.33, 157.51, 158.87
4a	105.65, 113.53, 113.75, 123.45, 124.17, 125.82, 125.96, 126.10, 126.24, 128.06, 128.28, 128.38, 128.55, 129.83, 130.02, 130.30, 130.60, 134.68, 136.10, 136.61, 137.01, 141.78, 141.90, 147.68, 147.99, 148.02, 148.18, 148.21, 149.90, 150.00, 152.18, 153.00, 153.56
4b	105.64, 113.54, 113.70, 123.45, 124.12, 124.92, 125.51, 125.80, 126.89, 128.00, 128.08, 128.56, 129.57, 129.86, 130.01, 130.56, 134.65, 134.87, 136.03, 136.64, 136.88, 137.85, 141.89, 147.34, 147.62, 147.99, 148.18, 148.90, 150.05, 150.38, 152.51, 152.85, 154.54
5a	110.33, 118.34, 118.53, 128.41, 128.76, 128.91, 129.01, 129.72, 130.69, 131.63, 132.25, 132.84, 133.06, 133.19, 133.24, 134.76, 134.82, 135.18, 135.34, 139.46, 140.16, 140.25, 141.32, 141.85, 141.91, 142.12, 143.01, 146.39, 146.65, 151.72, 151.95, 152.51, 152.86, 152.89, 153.49, 154.38, 154.59, 155.47, 156.60, 157.00, 157.14, 157.69, 161.89, 162.01, 162.27
5b	105.48, 113.60, 113.80, 123.22, 123.49, 123.73, 124.08, 124.38, 125.83, 126.16, 126.40, 126.77, 127.47, 128.04, 128.31, 128.55, 130.00, 130.39, 130.51, 130.57, 135.52, 136.31, 136.72, 136.98, 137.49, 138.09, 141.73, 141.99, 147.77, 147.83, 148.20, 148.82, 148.86 149.96, 150.85, 151.20, 152.15, 152.72, 153.12, 153.44, 154.21 156.39, 156.98, 157.38, 158.83

Table 6. ^1H NMR Data[a] for the Two Diastereoisomers *meso* ($\Lambda\Delta$) **4a** and *rac* ($\Lambda\Lambda$, $\Delta\Delta$) **4b** of $[(phen)_2Ru(H_2Pzbzim)Ru(phen)_2](ClO_4)_3\cdot 4H_2O$ in $(CD_3)_2SO$

proton[b]	**4a** ($\Lambda\Delta$)	**4b** ($\Lambda\Lambda$, $\Delta\Delta$)
	Bridging Ligand	
H(11)	7.59, 2H, 8.2	7.58, 2H, 8.1
H(12)	7.07, 2H, 7.6	7.08, 2H, 7.7
H(13)	6.54, 2H, 7.8	6.52, 2H, 7.6
H(14)	4.63, 2H, 8.3	4.71, 2H, 8.3
H(7)	8.22, 1H	8.19, 1H
	phen Ligands	
H(2)	5.95, 2H, 5.1	6.84, 2H, 5.2
	7.09, 2H, 5.3	6.93, 2H, 5.1
	7.12, 2H, 5.1	7.91, 2H, 5.2
	8.58, 2H, 5.2	8.70, 2H, 5.1
H(3)	6.58, 2H, 5.2 and 8.1	6.58, 2H, 4.9 and 8.1
	7.27, 2H, 5.3 and 8.2	7.26, 2H, 5.4 and 8.1
	7.33, 2H, 5.5 and 8.1	7.52, 2H, 5.2 and 8.2
	7.97, 2H, 5.5 and 8.0	8.10, 2H, 4.8 and 8.2
H(4)	8.02, 4H, 8.8	7.86, 4H, 8.1
	8.09, 2H, 8.9	8.09, 2H, 7.6
	8.34, 2H, 8.9	8.20, 2H, 7.0
H(5)	8.14, 2H, 8.2	8.26, 2H, 8.5
	8.48, 2H, 8.2	8.47, 2H, 8.3
	8.84, 4H, 8.2	8.50, 2H, 8.3
		8.75, 2H, 8.3

[a] For ^1H NMR data respectively: chemical shift (ppm), number of protons, *J* (Hz). H(2), H(4), and H(5) are doublets; H(3) is triplet or doublet of doublets. [b] For atom numbering scheme see Chart 1.

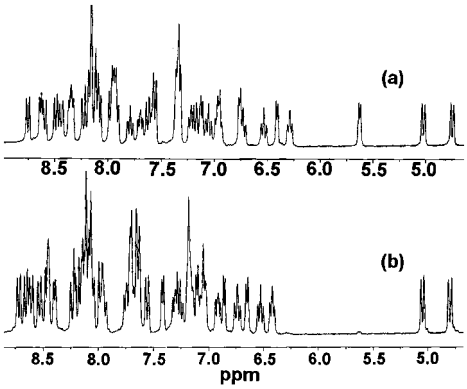

Figure 5. ^1H NMR spectra of the diastereoisomers **5a** (a) and **5b** (b) of the complex $[(bpy)_2Ru(H_2pzbzim)Ru(phen)_2](ClO_4)_3\cdot 4H_2O$ in $(CD_3)_2SO$: (a) enantiomeric pair ($\Lambda\Delta$, $\Delta\Lambda$); (b) enantiomeric pair ($\Lambda\Lambda$, $\Delta\Delta$).

tion processes are observed, of which the current height of the first wave, both in the CV and DPV, is twice that of the second or third, indicating that the first electron transfer process is bielectronic. The observed behavior is quite similar to that reported for ruthenium(II) complexes of other anionic electron-rich bridging ligands.[11b,c,g,14d,16a] It should be noted that while these electron transfers occur to the π-LUMO of bpy/phen, each of which can accept two electrons, the bridging ligand itself does not undergo reduction.

Table 7. ^1H NMR Data[a] for the Two Pairs of Enantiomers **5a** ($\Lambda\Delta$, $\Delta\Lambda$) and **5b** ($\Lambda\Lambda$, $\Delta\Delta$) of $[(bpy)_2Ru(H_2Pzbzim)Ru(phen)_2](ClO_4)_3\cdot 5H_2O$ in $(CD_3)_2SO$

proton[b]	**5a** ($\Lambda\Delta$, $\Delta\Lambda$)	**5b** ($\Lambda\Lambda$, $\Delta\Delta$)
	Bridging Ligand	
H(11)	7.63, 1H, 8.2	7.64, 1H, 8.0
H(11′)	7.56, 1H, 8.1	7.56, 1H, 8.1
H(12)	7.22, 1H, 7.2	7.26, 1H, 7.6
H(12′)	7.06, 1H, 7.7	7.18, 1H, 7.7
H(13)	6.73, 1H, 7.6	6.74, 1H, 7.8
H(13′)	6.54, 1H, 7.7	6.53, 1H, 7.8
H(14)	5.02, 1H, 8.4	5.05, 1H, 8.3
H(14′)	4.75, 1H, 8.2	4.80, 1H, 8.4
H(7)	8.16, 1H	8.11, 1H
	bpy Ligands	
H(3)	7.98, 1H, 8.4	8.05, 1H, 8.3
	8.11, 1H, 8.1	
	8.44, 1H, 8.1	8.47, 2H, 8.0
	8.49, 1H, 8.3	8.53, 1H, 8.1
H(4)	7.70, 1H, 7.8	7.66, 1H, 7.7
	7.79, 1H, 7.7	8.04−8.25, 3H[c]
	8.10, 2H, 7.7	
H(5)	6.29, 1H, 6.5	6.42, 1H, 6.5
	6.95, 1H, 6.5	6.92, 1H, 6.6
	8.35, 2H, 6.6	7.30, 1H, 6.5
		8.13, 1H, 6.7
H(6)	6.41, 1H, 5.0	6.86, 1H, 5.2
	6.77, 1H, 5.0	7.10, 1H, 5.1
	7.33, 1H, 5.1	7.41, 1H, 5.4
	7.58, 1H, 5.4	7.70, 1H, 5.3
	phen Ligands	
H(2)	5.63, 1H, 5.4	6.65, 1H, 5.4
	6.77, 1H, 5.0	7.04, 1H, 5.7
	7.12, 1H, 5.5	7.18, 1H, 5.3
	8.64, 1H, 5.1	8.40, 1H, 5.2
H(3)	7.18, 1H[c]	7.05, 1H[c]
	7.32−7.37, 3H[c]	7.63−8.25, 4H[c]
H(4)	7.90−8.30, 4H[c]	8.04−8.25, 4H[c]
H(5)	8.19−8.25, 2H[c]	8.04−8.25, 1H[c]
	8.60, 1H	8.61, 1H[c]
	8.76, 1H	8.65, 1H[c]
		8.72, 1H[c]

[a] For ^1H NMR data respectively: chemical shift (ppm), number of protons, *J* (Hz). [b] For atom numbering scheme see Chart 1. [c] Overlapping signals.

Absorption Spectra and Spectrophotometric Studies of Protonic Equilibria. Complexes **1**−**7** in acetonitrile exhibit a number of absorption bands in the spectral range 200−900 nm (Table 10). Two main regions can be distinguished: between 400 and 900 nm the spectra display two intense bands (ϵ =

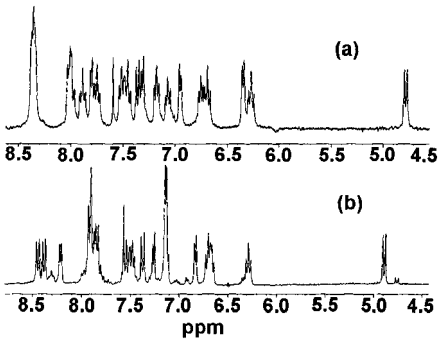

Figure 6. ^{1}H NMR spectra of the diastereoisomers **6a** (a) and **6b** (b) of the complex $[(bpy)_2Ru(H_2pzbzim)Ru(bpy)_2](ClO_4)_3\cdot 3H_2O$ in $(CD_3)_2SO$: (a) *meso* ($\Lambda\Delta$); (b) *rac* ($\Lambda\Lambda$, $\Delta\Delta$).

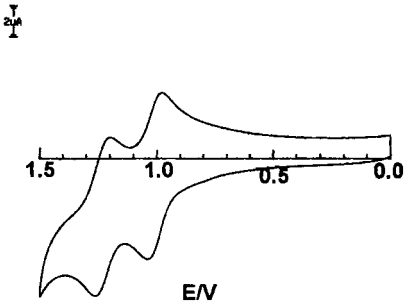

Figure 7. Cyclic voltammogram of **3** in acetonitrile exhibiting the redox couples $Ru^{II}Ru^{II}/Ru^{II}Ru^{III}$ and $Ru^{II}Ru^{III}/Ru^{III}Ru^{III}$.

Table 8. ^{1}H NMR Data[a] for the Two Diastereoisomers *meso* ($\Lambda\Delta$) **6a** and *rac* ($\Lambda\Lambda$, $\Delta\Delta$) **6b** of $[(bpy)_2Ru(H_2pzbzim)Ru(bpy)_2](ClO_4)_3\cdot 3H_2O$ in $(CD_3)_2SO$

proton[b]	**6a** ($\Lambda\Delta$)	**6b** ($\Lambda\Lambda$, $\Delta\Delta$)
	Bridging Ligand	
H(11)	7.35, 2H, 8.0	
H(12)	6.69, 2H, 7.6	6.70, 2H, 7.6
H(13)	6.27, 2H, 7.6	6.29, 2H, 7.6
H(14)	4.81, 2H, 8.1	4.90, 2H, 8.1
H(7)	7.53, 1H	7.57, 1H
	bpy ligands	
H(3)	8.05, 2H, 8.1	7.55, 2H, 8.0
	8.40, 6H, 7.8	7.93, 2H, 8.1
		8.39, 2H, 8.1
		8.45, 2H, 8.2
H(4)	7.47, 2H, 7.8	7.83, 2H, 7.8
	7.77, 2H, 7.6	7.88, 4H, 7.8
	7.90, 2H, 7.7	7.93, 2H, 7.8
	8.00, 2H, 7.7	
H(5)	6.80, 2H, 6.6	6.66, 2H, 6.7
	7.12, 2H, 6.6	7.13, 4H, 6.8
	7.20, 2H, 6.6	7.48, 2H, 6.8
	7.53, 2H, 6.5	
H(6)	6.34, 2H, 5.2	6.84, 2H, 5.3
	6.98, 2H, 5.2	7.13, 2H, 5.5
	7.33, 2H, 5.4	7.26, 2H, 5.4
	7.83, 2H, 5.3	8.22, 2H, 5.4

[a] For ^{1}H NMR data respectively: chemical shift (ppm), number of protons, *J* (Hz). H(3) and H(6) are doublets; H(4) and H(5) are triplets or doublets of doublets. [b] For atom numbering scheme see Chart 1.

6000−22000 M^{-1} cm^{-1}) due to the metal to ligand Ru(dπ) → bpy/phen (π^*) charge transfer transitions, while between 200 and 400 nm there are very intense bands (ϵ = 25000−120000 M^{-1} cm^{-1}) due to the intraligand $\pi-\pi^*$ transitions. Significantly, the absorption spectra exhibited by each pair of diastereoisomers **3a** and **3b**, **4a** and **4b**, and **5a** and **5b** are almost indistinguishable. On deprotonation of the bridging ligand, a

Table 9. Electrochemical Data[a] for the Mononuclear and Binuclear Ruthenium(II) Complexes in Acetonitrile

	oxidation[b]			reduction:[c] $E_{1/2}$(red), V		
compd	$E_{1/2}(1)$, V	$E_{1/2}(2)$, V	K_c			
1	0.89			−1.62	−1.90	
2	0.90			−1.64	−1.97	
3a	1.01	1.23	5.2×10^3	−1.52[d]	−1.90	−2.06
3b	1.01	1.23	5.2×10^3	−1.50[d]	−1.92	−2.06
4a	1.02	1.23	3.5×10^3	−1.47[d]	−1.93	−2.07
4b	1.01	1.25	1.1×10^4	−1.42[d]	−1.90	−2.10
5b	1.00	1.24	1.1×10^4	−1.48[d]	−1.90	−2.08
6a	0.63[e]	0.96[f]	3.8×10^5			
6b	0.64[e]	0.97[f]	3.8×10^5			

[a] All the potentials are referenced against Ag/AgCl electrode with $E_{1/2}$ = 0.36 V for F_c/F_c^+ couple. [b] Reversible electron-transfer process with a Pt working electrode. [c] $E_{1/2}$ values obtained from differential pulse voltammograms using a glassy carbon electrode at a scan rate of 20 mV s^{-1}. [d] Two overlapping one-electron-transfer reactions. [e] Quasi-reversible process, $E_{pa} - E_{pc}$ = 90 mV at υ = 200 mV s^{-1}. [f] Quasi-reversible process, $E_{pa} - E_{pc}$ = 120 mV at υ = 200 mV s^{-1}.

Table 10. Absorption Spectral Data for the Mononuclear and Binuclear Ruthenium(II) Complexes

compd[a]	λ_{max}, nm(ϵ, $M^{-1}cm^{-1}$)
1	502 (9480), 447 (5880), 331 (32 100), 311 (50 300), 294 (74 000), 243 (47 000)
2	496 (12 600), 445 (10 700), 312 (48 300), 265 (86 400), 223 (90 100)
3a	494 (12 450), 436 (9070), 330 (44 300), 311 (53 360), 294 (97 500), 242 (73 000)
3b	494 (12 600), 435 (9000), 330 (42 800), 310 (5500), 295 (96 000), 240 (75 100)
4a	480 (17 970), 435 (20 030), 320 (40 050), 265 (116 000), 220 (124 000)
4b	480 (17 400), 435 (19 800), 320 (36 500), 265 (110 000), 220 (117 000)
5a	485 (15 100), 435 (15 300), 320 (36 600), 290 (60 000), 270 (77 000), 225 (85 000)
5b	485 (15 000), 435 (15 600), 320 (35 400), 290 (62 000), 270 (76 000), 225 (87 000)
6a	527 (10 700), 470 (9500), 322 (43 800), 296 (85 000), 241 (75 000)
6b	528 (11 200), 470 (9100), 320 (45 000), 295 (84 300), 240 (74 600)
7	513 (14 800), 455 (15 600), 321 (45 000), 265 (113 000), 224 (125 000)

[a] In MeCN.

substantial red shift of the MLCT bands takes place. Thus, the two absorption maxima at 447 and 502 nm for $[(bpy)_2Ru(H_3pzbzim)]^{2+}$ are shifted to 508 and 530 nm in $[(bpy)_2Ru(Hpzbzim)]$; similarly, the peaks at 436 and 494 nm for $[\mathbf{3}]^{3+}$ are shifted to 470 and 527 nm in $[\mathbf{6}]^+$.

The influence of pH on the absorption spectra of **3**−**5** (shown in Figure 8) has been studied quantitatively by performing spectrophotometric titrations of the complexes in acetonitrile−water (3:2) solutions over the pH range 2−12. Typically for **3** (Figure 8a), the spectrum remains unchanged in the low pH range 2.0−3.5. However, as the pH is increased from 3.5 to 8.8, the absorption maxima at 435 and 478 nm are progressively shifted to 445 and 485 nm with an isosbestic point occurring at 488 nm; on further raising of the pH, the bands are additionally red-shifted through a second isosbestic point at 502 nm till the maxima at 465 and 515 nm are reached at pH 12.0, beyond which no further change occurs. The appearance of two successive isosbestic points with the increase of pH provides a good indication of the involvement of two successive depro-

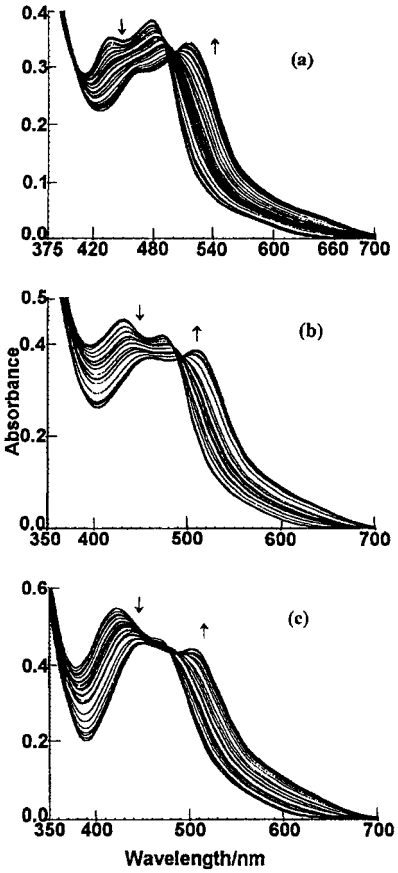

Figure 8. pH dependence of the absorption spectra of $[(bpy)_2Ru(H_2pzbzim)Ru(bpy)_2]^{3+}$ (a), $[(bpy)_2Ru(H_2pzbzim)Ru(phen)_2]^{3+}$ (b), and $[(phen)_2Ru(H_2pzbzim)Ru(phen)_2]^{3+}$ (c) in acetonitrile−water (3:2) solution. The pH of the solutions has been varied between 1 and 12.

tonation equilibria.[42] Indeed, the presence of three complex species in the equilibrium mixture has been verified by analyzing the spectrophotometric titration data by a graphical method due to Coleman et al.[43] Taken together, the acid−base equilibria of **3** can be described as

$$[(bpy)_2Ru(H_2pzbzim)Ru(bpy)_2]^{3+} \underset{H^+}{\overset{K_{11}}{\rightleftharpoons}} [(bpy)_2Ru(Hpzbzim)Ru(bpy)_2]^{2+} \underset{H^+}{\overset{K_{12}}{\rightleftharpoons}} [(bpy)_2Ru(pzbzim)Ru(bpy)_2]^{+} \quad (2)$$

The individual pK_{ij} values have been evaluated from the two segments of the spectrophotometric titration data at pH 3.5−8.8 and 8.8−12.0 using eq 3,

$$\mathrm{pH} = pK_{ij} - \log \frac{A - A_0}{A_f - A} \quad (3)$$

where A_0, A_f, and A refer to the absorbances at the initial, final, and intermediate pH values at a given wavelength.

A comparison of the pH vs absorbance curves for **5** (Figure 8b) with those of **3** (Figure 8a) and **4** (Figure 8c) reveals that the change in pattern of the spectral profile of **5** is intermediate between those of **3** and **4**. This suggests that although the intensities of the MLCT bands are controlled by the $Ru(ppy)_2^{2+}$ chromophores, the pK values of the bridging ligand get far less affected due to the variation of the chromophores. Indeed, the pK values of the three compounds (given below) are in good agreement with each other.

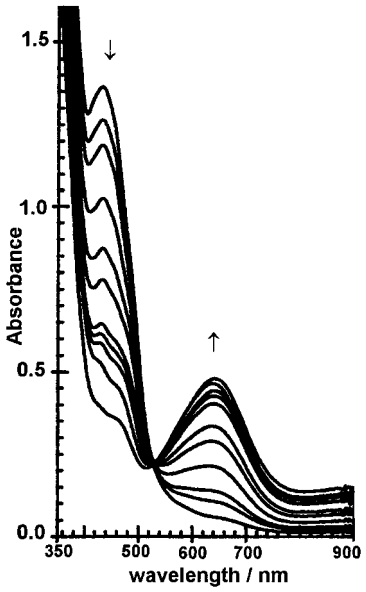

Figure 9. Change in the absorption spectra of $[(bpy)_2Ru(H_2pzbzim)Ru(bpy)_2]^{3+}$ on oxidation with cerium(IV) in acetonitrile−water (3:2) solution.

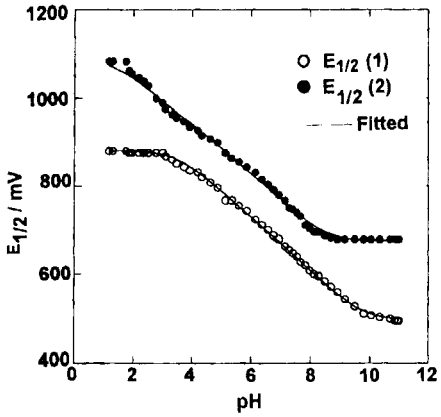

Figure 10. Experimental (○, ●) and simulated (—) plots for the variations of the redox potentials $E_{1/2}(1)$ and $E_{1/2}(2)$ with pH for $[(bpy)_2Ru(H_2pzbzim)Ru(bpy)_2]^{3+}$ in acetonitrile−water (3:2) solution.

pK_{11}: 7.95(5) (**3**), 7.90(5) (**4**), 7.75(5) (**5**)

pK_{12}: 9.75(5) (**3**), 9.80(5) (**4**), 9.75(5) (**5**)

It should be noted that the benzimidazole NH protons in H_3-pzbzim itself are too weakly acidic for determination of their pK values (>12). Therefore, p$K_{11} \approx 7.9$ and p$K_{12} \approx 9.8$ in the complexes demonstrate severalfold increases in the acidity of these NH protons consequent to metal binding.

The generation of ruthenium(III) species by the chemical oxidation of the ruthenium(II) complexes with cerium(IV) in acetonitrile−water (3:2) solution has also been studied spectrophotometrically. The spectral changes that occur during the redox titration of **3** (Figure 9) show that the more intense $Ru^{II}d\pi \rightarrow \pi^*$(bpy) MLCT band gradually disappears at the expense of the formation of the less intense π(bridging ligand) → Ru^{III}-$(t_{2g}^5)d\pi$ LMCT band. As compared to the absorption peaks for the MLCT bands in **3** (436, 494 nm), the LMCT band in the

(42) (a) Long, C.; Vos, J. G. *Inorg. Chim. Acta* **1984**, *89*, 125. (b) Crutchley, R. J.; Kress, N.; Lever, A. B. P. *J. Am. Chem. Soc.* **1983**, *105*, 1170.
(43) Coleman, J. S.; Varga, L. P.; Mastin, S. H. *Inorg. Chem.* **1970**, *9*, 1013.

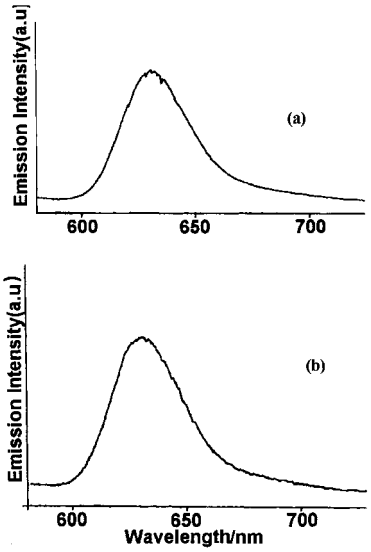

Figure 11. Emission spectra of the diastereoisomers **4a** (a) and **4b** (b) of $[(phen)_2Ru(H_2pzbzim)Ru(phen)_2](ClO_4)_3 \cdot 4H_2O$ in methanol−ethanol (1:4) frozen glass at 77 K.

Scheme 3

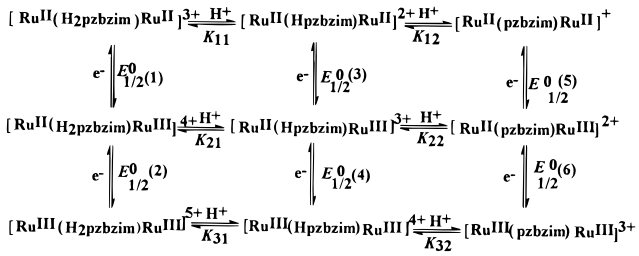

oxidized diruthenium(III) species is observed at a considerably higher wavelength (640 nm).

Proton-Coupled Electron Transfer Reaction Equilibria. As already noted, on coordination to the metal centers the NH protons of the bridging ligand become appreciably acidic. Consequently, redox potentials of the complexes should be tunable as a function of pH of the medium. To study this, the redox potentials of **3** have been monitored in the pH range 1−12 in 3:2 (v/v) acetonitrile−aqueous solution. It should be noted that the redox potentials of **3** in pure acetonitrile, as reported earlier, differ from those obtained in the aqueous acetonitrile medium due to solvent effect. The extent of the difference can be judged by comparing the $E_{1/2}$ value of the ferrocene/ferrocenium couple in acetonitrile (0.36 V) vis-à-vis the 3:2 acetonitrile−water mixture (0.26 V).

Complex **3** over the entire pH range (1−12) exhibits two well-resolved redox couples in the potential window 0−2 V. The variations of $E_{1/2}(1)$ and $E_{1/2}(2)$ with respect to pH are shown in Figure 10. It may be noted that when the pH is either less than 3.5 or greater than 9.8, the $E_{1/2}(1)$ values remain pH-invariant, indicating that in these regions the electron-transfer processes are not accompanied by proton transfer. Over the pH range 3.5−9.8, the slope of the plot of $E_{1/2}(1)$ vs pH is close to −60 mV/pH. In the $E_{1/2}(2)$ vs pH plot also the invariance of $E_{1/2}$ with pH is observed when the pH is either less than 1.4 or greater than 8.5. Again, in the intermediate pH range, between 1.4 and 8.5, the slope is close to −60 mV/pH. A closer examination of the $E_{1/2}(2)$ vs pH plot (Figure 10) reveals the presence of two successive equilibria, each involving one-proton and one-electron transfers; in the $E_{1/2}(1)$ vs pH plot, however, these two processes are merged. The proton and electron-transfer reactions encompassing the entire pH range may be described by the reaction equilibria shown in Scheme 3.

The relations between the redox potentials and the acid dissociation constants of the complex species are given by the equations

$$E_{1/2}(1) = E_{1/2}^{\circ}(1) + 0.059 \log \frac{[H^+]^2 + K_{11}[H^+] + K_{11}K_{12}}{[H^+]^2 + K_{21}[H^+] + K_{21}K_{22}} \quad (4)$$

$$E_{1/2}(2) = E_{1/2}^{\circ}(1) + 0.059 \log \frac{[H^+]^2 + K_{21}[H^+] + K_{21}K_{22}}{[H^+]^2 + K_{31}[H^+] + K_{31}K_{32}} \quad (5)$$

where $E_{1/2}^{\circ}(1)$ and $E_{1/2}^{\circ}(2)$ are the standard redox potentials of the couples $Ru^{II}Ru^{II}/Ru^{II}Ru^{III}$ and $Ru^{II}Ru^{III}/Ru^{III}Ru^{III}$, respectively. Nonlinear least-squares analysis of the experimental data have provided the best fit curves (shown in Figure 9) with the following pK values: $pK_{11} = 7.7$ and $pK_{12} = 9.8$ for $Ru^{II}Ru^{II}$; $pK_{21} = 3.5$ and $pK_{22} = 8.6$ for $Ru^{II}Ru^{III}$; $pK_{31} = 1.4$ and $pK_{32} = 3.7$ for $Ru^{III}Ru^{III}$. The $E_{1/2}^{\circ}$ values of all of the protonated/deprotonated redox couples involved in Scheme 3 are $E_{1/2}^{\circ}(1) = 0.88$ V; $E_{1/2}^{\circ}(2) = 1.08$ V, $E_{1/2}^{\circ}(3) = 0.63$ V, $E_{1/2}^{\circ}(4) = 0.74$ V; $E_{1/2}^{\circ}(5) = 0.50$ V; $E_{1/2}^{\circ}(6) = 0.68$ V.

As expected, stepwise deprotonation of the bridging ligand progressively shifts the redox potentials to less positive values. The extent of shift in potentials on passing from the fully protonated state to the fully deprotonated state is almost identical for the couples $Ru^{II}Ru^{II}/Ru^{II}Ru^{III}$ ($E_{1/2}^{\circ}(1) - E_{1/2}^{\circ}(5) = 0.38$ V) and $Ru^{II}Ru^{III}/Ru^{III}Ru^{III}$ ($E_{1/2}^{\circ}(2) - E_{1/2}^{\circ}(6) = 0.40$ V). When the electron transfer processes are not accompanied by proton transfer, the differences between the potentials of $Ru^{II}Ru^{III}/Ru^{III}$-Ru^{III} and $Ru^{II}Ru^{II}/Ru^{II}Ru^{III}$ couples in the fully protonated form ($E_{1/2}^{\circ}(2) - E_{1/2}^{\circ}(1) = 0.20$ V) and in the fully deprotonated form ($E_{1/2}^{\circ}(6) - E_{1/2}^{\circ}(5) = 0.18$ V) are similar. For the monoprotonated species the difference in the $E_{1/2}^{\circ}$ values for the above-mentioned couples ($E_{1/2}^{\circ}(4) - E_{1/2}^{\circ}(3) = 0.11$ V) is relatively less.

Of particular interest are the pK values determined spectrophotometrically as well as electrochemically. The values of pK_{11} (7.95 ± 0.05) and pK_{12} (9.75 ± 0.05) obtained by the spectrophotometric method compare reasonably well with the values 7.7 and 9.8 obtained by the electrochemical method. It may be noted that the differences in the pK values of the two benzimidazole protons in the isovalent $Ru^{II}Ru^{II}$ ($pK_{12} - pK_{11} = 2.1$) and $Ru^{III}Ru^{III}$ ($pK_{32} - pK_{31} = 2.3$) states are much less compared to that in the mixed-valence $Ru^{II}Ru^{III}$ state ($pK_{22} - pK_{21} = 5.1$). The large difference observed in the mixed-valence state gives a clear indication of the valence-trapped situation, that is, class II behavior.

Luminescence Spectra. The emission spectral behavior of complexes **1**−**7** has been studied at room temperature and 77 K using acetonitrile or methanol−ethanol (1:4) solutions or methanol−ethanol glass. The spectra recorded in methanol−ethanol solutions are of better quality than those obtained in acetonitrile. Further, relative to the solution spectra, the emission spectra in frozen glass are sharper and considerably more intense. Table 11 summarizes the emission peaks, quantum yields, and excited state redox potentials of the complexes. The emission spectra of the diastereoisomers **4a** and **4b** (Figure 11) exhibit identical features, as is the case with **3a** and **3b** and with **5a** and **5b**. The spectra exhibited by the mononuclear complexes are basically similar to their binuclear analogues.

Table 11. Emission Spectral Data and Excited State Redox Properties of the Ruthenium(II) Complexes

	emission[a]						
	298 K		77 K		E_{oo},[b]	$E^*_{(ox)}$,[c]	$E^*_{(red)}$,[d]
compd	λ_{nm}	φ	λ_{nm}	φ	V	V	V
1	680	3.5×10^{-3}	640	0.072	1.94	−1.05	0.32
2	660	3.8×10^{-3}	635	0.080	1.95	−1.05	0.31
3a	675	5.6×10^{-3}	640	0.075	1.94	−0.93, −0.71	0.42
3b	675	5.8×10^{-3}	640	0.078	1.94	−0.93, −0.71	0.44
4a	670	6.0×10^{-3}	630	0.081	1.97	−0.95, −0.74	0.50
4b	670	5.95×10^{-3}	630	0.080	1.97	−0.96, −0.72	0.55
5a	675	5.7×10^{-3}	635	0.076	1.95	−0.94, −0.73	0.46
5b	675	5.6×10^{-3}	635	0.075	1.95	−0.95, −0.71	0.47

[a] In 1:4 methanol−ethanol mixture. [b] Taken as the emission energy maximum at 77 K. [c] $E^*_{(ox)} = E_{1/2}(ox) - E_{oo}$. [d] $E_{(red)} = E^*_{oo} - E_{1/2}(red)$.

The ruthenium(II) complexes, on excitation at the wavelengths where their two MLCT absorption maxima are observed, exhibit two to three luminiscent bands in the range 500−800 nm. The peak of the longer wavelength band, which lies between 660 and 680 nm at 300 K, remains unchanged with the energy of excitation radiation. However, the peak positions of the luminescent bands observed at 500−570 nm are affected by the irradiation wavelength; they undergo a blue shift on lowering of the excitation wavelength. The emission band occurring at the lower energy has the characteristic of emission from the ^{3}MLCT excited state, which corresponds to a spin-forbidden Ru → bpy/phen transition.[44,45] In solution, at room temperature, all of the complexes are weak emitters with their quantum yields ranging from 3×10^{-3} to 7×10^{-3}. On the other hand, in frozen glass, the longer wavelength peak observed at 635−640 nm shows a significant increase of quantum yield, 0.07−0.09. The blue shift of the emission band on passing from fluid solution to rigid matrix is typical of MLCT emitters[44−46] and is mainly due to the inability of frozen sovent to reorganize around the excited molecule.[47] The enhancement of intensity on lowering of temperature results from slowing down of radiationless transitions, including thermally activated population of short-lived, upper-lying excited states.[48]

The origin of the emission band(s) in the range 500−570 nm is not clear. It could be due to either emission from the ^{1}MLCT state or the ligand-centered (bpy/phen) excited state (singlet or triplet). In light of known facts, metal-perturbed ligand-centered emission appears to be more plausible.[49]

One important aspect of this study has been to examine the effect of pH on properties of the complexes, including their fluorescence spectral behavior. While the intervalence transfer transition of the electrochemically generated $Ru^{II}Ru^{III}$ species as well as the fluorescence spectra of the ruthenium(II) complexes as a function of pH will be the subject of a future report, we report here that all of the deprotonated compounds derived from **1**−**5** do not luminesce either in solution or in frozen glass. This indicates that, by varying the bulk parameter pH, "on/off" switching of fluorescence can be brought about in these systems. Clearly, the photoexcited deprotonated species get spontaneously quenched[50] due to the migration of electrons from the negatively charged benzimidazole moieties.

Acknowledgment. K.N. thanks the Council of Scientific and Industrial Research, India for funding this work. Our thanks are also due to Dr. Kausik K. Nanda of Drexel University for helpful assistance.

Supporting Information Available: Tables of crystal data and structure refinement (Table S1), anisotropic thermal parameters (Tables S2), hydrogen atom coordinates (Table S3) and complete bond lengths and angles (Table S4); figures of ^{1}H NMR spectrum of **4** (Figure S1), COSY spectra of **4a** and **4b** (Figure S2(a), S2(b)), and ^{1}H NMR spectrum of **5** (Figure S3). This material is available free of charge via the Internet at http://pubs.acs.org.

IC980564S

(44) Juris, A.; Balzani, V.; Barigelletti, F.; Campagna, S.; Belser, P.; von Zelewsky, A. *Coord. Chem. Rev.* **1988**, *84*, 85.
(45) Kalyanasundaram, K. *Photochemistry of Polypyridine and Porphyrin Complexes;* Academic Press: London, 1992.
(46) Meyer, T. J. *Pure Appl. Chem.* **1986**, *58*, 1193.
(47) Lumpkin, R. S.; Meyer, T. J. *J. Phys. Chem.* **1986**, *90*, 5307.
(48) (a) Demas, J. N.; Crosby, G. A. *J. Am. Chem. Soc.* **1971**, *93*, 2841. (b) Demas, J. N.; Taylor, D. G. *Inorg. Chem.* **1979**, *18*, 3177.
(49) (a) Belser, P.; von Zelewsky, A.; Juris, A.; Barigelletti, F.; Tucci, A.; Balzani, V. *Chem. Phys. Lett.* **1982**, *89*, 101. (b) Sprouse, S.; King, K. A.; Spellane, P. J.; Watts, R. J. *J. Am. Chem. Soc.* **1984**, *106*, 6647. (c) Maestri, M.; Sandrini, D.; Balzani, V.; Maeder, U.; von Zelewsky, A. *Inorg. Chem.* **1987**, *26*, 1323.
(50) Fabbrizzi, L.; Poggi, A. *Chem. Soc. Rev.* **1995**, 197.